Gondwana Research 28 (2015) 288–310

Contents lists available at ScienceDirect

Gondwana Research

journal homepage: www.elsevier.com/locate/gr

Basement nature and origin of the Junggar terrane: New zircon U–Pb–Hf isotope evidence from Paleozoic rocks and their enclaves

Xing-Wang Xu [a,b,*], Xian-Hua Li [a], Neng Jiang [a], Qiu-Li Li [a], Xun Qu [c], Yue-Heng Yang [a], Gang Zhou [c], Lian-Hui Dong [c]

[a] Key Laboratory of Mineral Resources, Institute of Geology and Geophysics, Chinese Academy of Sciences, Beijing 100029, China
[b] Xinjiang Research Center for Mineral Resources, Chinese Academy of Sciences, Urumqi 830011, China
[c] Xinjiang Bureau of Geology and Mineral Resources, Urumqi, Xinjiang 830000, China

ARTICLE INFO

Article history:
Received 31 October 2013
Received in revised form 13 March 2014
Accepted 14 March 2014
Available online 13 April 2014

Handling Editor: W.J. Xiao

Keywords:
Zircon U–Pb–Hf isotope evidence
Basement nature
Origin
The Junggar terrane
Southern Laurentia

ABSTRACT

The question of whether the Junggar terrane in the central area of the Central Asian Orogenic Belt (CAOB) has a Precambrian basement is one of the hottest topics surrounding the tectonic evolution of the CAOB. Recent work shows that the Central Tianshan range has a Mesoproterozoic–Neoproterozoic basement. Here, we reported the SIMS U–Pb age and Hf isotopes of zircons from newly discovered dioritic gneiss and magnetite quartzite enclaves and their host diorite dike in the Taheir area, deformed Ordovician conglomerate in the Dazigou area, and mica gneiss relicts and their host granite in the Shuangchagou area in the Junggar terrane. The results reveal the following evidence: 1) the dioritic gneiss was metamorphosed from 2.52 Ga diorite at approximately 1.88 Ga, the magnetite quartzite interlayered with hornblende–plagioclase gneiss layers has an age of approximately 1.92 Ga, and the inherited zircons from the diorite TH4-6 contain three zircon populations with upper intercept ages of approximately 3.06 Ga, 1.98 Ga and 1.89 Ga; 2) the sienna and colorless zircon populations from the conglomerate reveal two magmatic rocks with ages of approximately 1.86 Ga and 0.94 Ga; and 3) the magmatic zircons that form mica gneiss have T_{DMC} and T_{DM2} ages ranging from 1.2 Ga to 2.08 Ga, and the inherited zircons from the mica gneiss and granite in the Shuangchagou area contain five zircon populations with upper intercept ages of approximately 2.48 Ga, 1.80 Ga, 1.47 Ga,1.14 Ga and 0.96 Ga.

By combining the published U–Pb ages and Hf isotope data of zircons from the Junggar terrane, it is suggested that the Junggar terrane has three Precambrian basement units, including the 2.1–1.7 Ga Taheir–Kalamaili–Dazigou reworked Archean crust, the 2.5–1.8 Ga Shuangchagou–Luliang crust and the 1.86–1.7 Ga Tianshan crust between the Aermantai subduction zone and south Tianshan suture. There is also the possibility of a 1.92 Ga quartzite formation in the Taheir area, 1.9–1.8 Ga orogen along the Taheir–Dazigou–Shuangchagou line, 1.47–1.40 Ga granitoids in the Shuangchagou–Xingxingxia area, 1.2–1.0 Ga magmatic rocks in the Dazigou–Shuangchagou area, a massive 1.0–0.9 Ga magmatic–metamorphic rock belt along the Tianshan range and in the Shuangchagou–Dazigou area, and 0.8–0.6 Ga magmatic rocks in the Taheir, Dazigou, Shuangchagou and Baluntai area. Regular arrangements of the three basement units and various sedimentary, magmatic and metamorphic belts indicate that the Precambrian Junggar terrane was possibly split from southern Laurentia near the Lake Superior region at 1.1 Ga and adjacent to the Caborca region at 1.0–0.6 Ga.

1. Introduction

The Junggar terrane, which is situated between the Zaisan–Erqis–Main Mongolian Lineament–Okhotsk suture and Tarim craton and occupies the central area of the Central Asian Orogenic Belt (CAOB, also known as Altaids) (Fig. 1a), is one of the important tectonic units in the evaluation and examination of the greatest continental accretion on earth. However, the basement nature of the Junggar terrane has long been controversial, and two models have been proposed for its genesis. One model suggests that the Junggar terrane has pre-Cambrian basement as its continental block (e.g. Zhang et al., 1984; Watson et al., 1987; Xiao et al., 1992; Zhang et al., 1993; He et al., 1994; Li et al., 2000; Charvet et al., 2001; Xu et al., 2003; Zhao et al., 2003; Buslov et al., 2004; Xu and Ma, 2004; Charvet et al., 2007; Dong et al., 2009; Bazhenov et al., 2012; Choulet et al., 2012; Zhang et al., 2013). The other model proposes that the Junggar terrane has a basement of Paleozoic oceanic crust (e.g., Carroll et al., 1990; Dobretsov et al., 2003; Windley et al., 2007; Zheng et al., 2007) or oceanic island arc complexes (e.g., Coleman, 1989; Chen and Jahn,

* Corresponding author at: Key Laboratory of Mineral Resources, Institute of Geology and Geophysics, Chinese Academy of Sciences, Beijing 100029, China. Tel.: +86 10 82998198; fax: +86 10 62010846.
E-mail address: xuxw@mail.iggcas.ac.cn (X.-W. Xu).

http://dx.doi.org/10.1016/j.gr.2014.03.011
1342-937X/

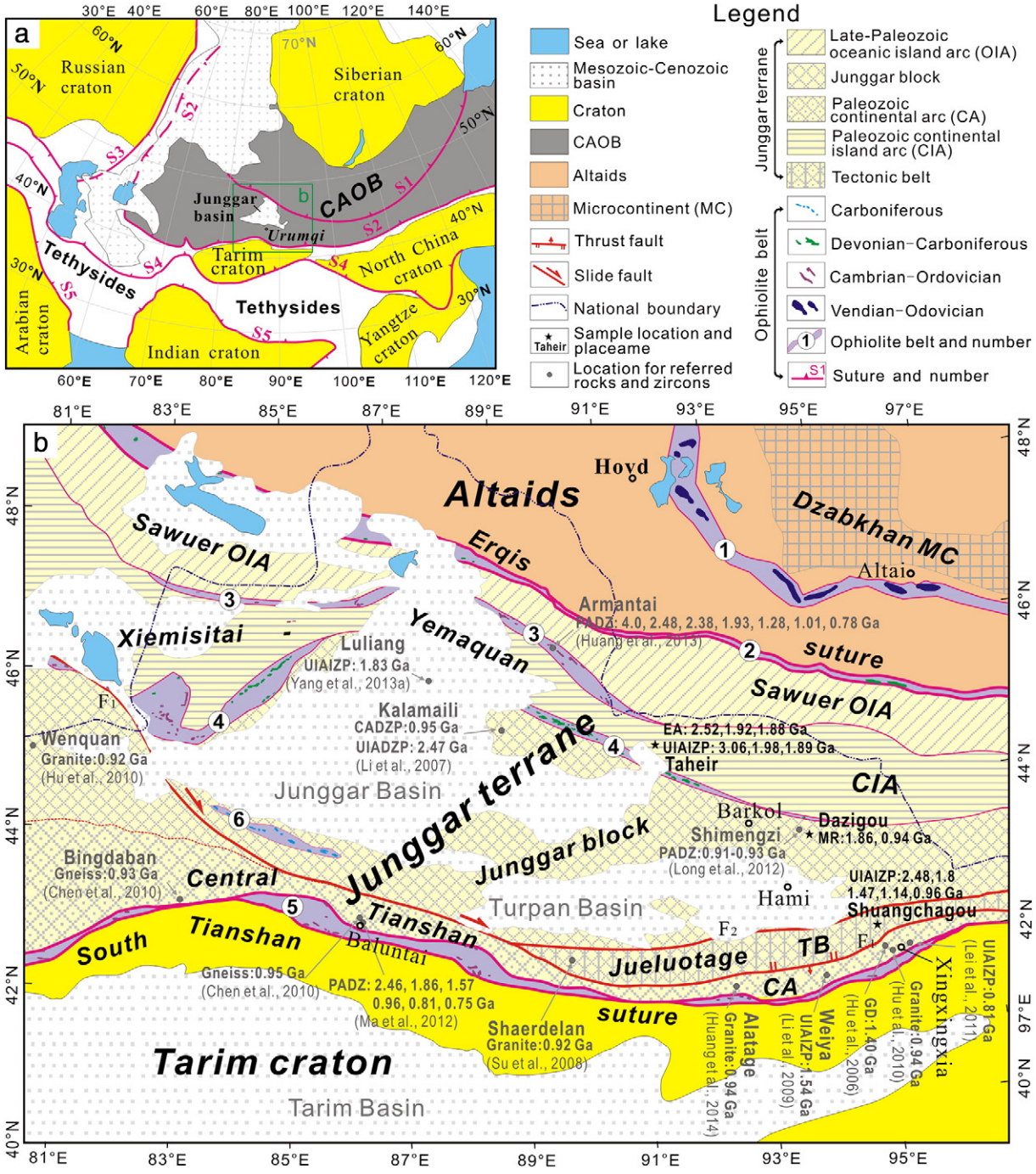

Fig. 1. Location (a) and Paleozoic tectonic units (b) of the Junggar terrane. Panel a is revised from Sengör and Natal'in (1996), Jahn et al. (2000) and Xiao et al. (2008, 2010), and panel b is revised from Dong et al. (2009) and Xu et al. (2013). Sutures in panel a: Zaisan–Erqis–the Main Mongolian Lineament–Okhotsk suture (S1), Kazakhstan–S. Tienshan–Xra Moron–Changchun suture (S2), Ural suture (S3), W. Kunlun–Altyn–Qilian–Qinling–Dabie suture (S4), Alpine–Himalayan suture (S5). Ophiolite belts in panel b: ①Hovd-Drive–Khantai-Shir ophiolite belt, ②Erqis ophiolite belt, ③ Hongguleleng–Aermantai ophiolite belt, ④ Tangbale–Darbute–Kalamaili ophiolite belt, ⑤ South Central Tianshan ophiolite belt, and ⑥ Bayinggou ophiolite belt. Ophiolites epochs are from Xiao et al. (2008), Buchan et al. (2002), and the references therein. F_1: Jinghe–Aaikkudug–Shaquanzi fault, F_2: Dacaotan fault. CA: continental arc; CAOB: Central Asian Orogenic Belt; CIA: continental island arc; MC: micro-continent; OIA: oceanic island arc; CADZP: concordia age of detrital zircon population; EMZ: euhedral magmatic zircon; GD: granodiorite; EA: enclave age; MR: magmatic rock; PADZ: peak age of detrital zircons; UIADZP: upper intercept age of detrital zircon population; UIAIZP: upper intercept age of inherited zircon population. Gray dots show sample locations of the published data. Black stars show sample locations of this study.

2004) as the juvenile crust (Jahn et al., 2000, 2004) of the Altaid Paleozoic rocks (e.g., Sengör et al., 1993; Sengör and Natal'in, 1996; Allen and Vincent, 1997; Filippova et al., 2001; Xiao et al., 2004a, 2004b, 2008, 2009a, 2009b, 2010a, 2010b, 2013). The main reason for the controversy is that no reliable Precambrian basement rocks have been identified because the area is covered by Paleozoic–Mesozoic–Cenozoic sedimentary rocks. Recent work shows that the Central Tianshan range has a Mesoproterozoic–Neoproterozoic basement with abundant 1.0–0.9 Ga and 1.4 Ga granitoids and gneiss (e.g., Hu et al., 2006; Su et al., 2008; Chen et al., 2009; Q.G. Li et al., 2009; Hu et al., 2010; Lei et al., 2011; Huang et al., 2014), and that a great number of Archean–Proterozoic detrital and inherited zircons occur throughout the Junggar terrane from the Central Tianshan at south to the east Junggar at north (e.g., Li et al., 2007; He et al.,

2012b; Long et al., 2012; Ma et al., 2012; Huang et al., 2013; Xu et al., 2013). In this contribution, we report on the U–Pb–Hf isotopes of zircons from the newly discovered dioritic gneiss and magnetite quartzite enclaves and their host diorite dike in the Taheir area, deformed Ordovician conglomerate in the Dazigou area, and mica gneiss relicts and their host granite in the Shuangchagou area in the Junggar terrane. In addition, we discuss the basement nature and origin of the Junggar terrane.

2. Paleozoic tectonic framework of the Junggar terrane

The Paleozoic Junggar terrane is bounded by the Erqis suture in the north and South Tianshan suture in the south (Fig. 1b; e.g., Allen and Vincent, 1997; Badarch et al., 2002; Chen and Jahn, 2004; Dong et al., 2009; Xiao et al., 2009b; Wong et al., 2010; Han et al., 2010; He et al., 2012b). The Erqis suture and South Tianshan suture are segments of the Zaisan–Erqis–Main Mongolian Lineament–Okhotsk suture and the Main Ural–Turkestan–South Central Tianshan–Solonker–Xra Moron–Changchun suture, respectively. The Zaisan–Erqis–Main Mongolian Lineament–Okhotsk suture, represented by a Silurian–Carboniferous ophiolite belt (e.g., Zhang et al., 2003; Kröner et al., 2007; Wong et al., 2010), likely marks the final closure line of the Paleo-Asian Ocean between the Altaid–Mongolia terrane and Kazakhstan–Junggar terrane (Fig. 1a; e.g., Glorie et al., 2011; Xu et al., 2013). The successive northward subduction of the Paleo-Asian Ocean produced the Altaids, which were separated by sequential ophiolites with ages of 1020 to 325 Ma, from the present margin of the Siberian craton to southern Siberia and northern Mongolia as well as to the main Mongolian Lineament in the Carboniferous (Windley et al., 2002; Kröner et al., 2007). The Main Ural–Turkestan–South Central Tianshan–Solonker–Xra Moron–Changchun suture zone represents the final suture of the Ural–Turkestan–South Tianshan Ocean between the Kazakhstan–Junggar–Southern Mongolia terranes and Tarim–North China cratons (Windley et al., 1990; Allen et al., 1992; Gao et al., 1998; Xiao et al., 2003; Solomovich, 2007; Wu et al., 2007; Biske and Seltmann, 2010). The South Central Tianshan ophiolite belts have ages of 600–590 Ma in the Sinian Dalubayi area (Yang et al., 2005), 516 Ma in the Hongliuhe area (Zhang and Guo, 2008) and 533 Ma in the Yueyashan–Xichangjing area (Ao et al., 2012). Both the Erqis Ocean (a segment of the Paleo-Asian Ocean) and the South Tianshan Ocean (a segment of the Urals–Turkestan–South Tianshan–Solonker Ocean) were possibly opened before the Ordovician (Wong et al., 2010; Long et al., 2011; Xu et al., 2013) and closed during the Carboniferous–Early Permian (e.g. Gao et al., 2009; Xiao et al., 2009a; Biske and Seltmann, 2010; Han et al., 2010; Gao et al., 2011; Glorie et al., 2011; Han et al., 2011; Liu et al., 2012; Su et al., 2012; Li et al., 2014).

The Paleozoic Junggar terrane around the Junggar basin consists of the NW-trending Devonian–Carboniferous Sawuer oceanic island arc, Cambrian–Ordovician Hongguleleng–Aermantai ophiolite belt, Paleozoic Xiemisitai–Yemaquan magmatic arc, Devonian–Carboniferous Tangbale–Darbute–Kelameili ophiolite belt, Junggar block, Jiaoluotage tectonic belt and Paleozoic Central Tianshan magmatic arc from the north to south (Fig. 1b).

The Sawuer oceanic island arc to the south of the Erqis suture is characterized by the occurrence of Devonian adakites, porphyry Cu–Au deposits and Nb-enriched basalts, and it developed on an Ordovician–Devonian juvenile crust (Zhang et al., 2004, 2006; Dong et al., 2009; Z. C. Zhang et al., 2009). The Hongguleleng–Aermantai ophiolite belt has ages of 503–481 Ma (Jian et al., 2003; Xiao et al., 2006). The Yemaquan magmatic arc is an Ordovician continental arc that changed to continental island arc after 432 Ma (Xu et al., 2013), and is characterized by the occurrence of porphyry Cu–Mo deposits in the Qiongheba area (Dong et al., 2009; Qu et al., 2009; Du et al., 2010) and abundant alkaline granites associated with Sn deposits in the Kelameili area (Lin et al., 2007; Tang et al., 2007). The Tangbale–Darbute–Kelameili ophiolite belts consist of a 508–470 Ma Tangbale ophiolite belt in the western segment (Kwon et al., 1989; Zhang, 1997), 414–398 Ma Darbute ophiolite belt in the middle segment (Xu et al., 2006; Xia et al., 2007) and 403–336 Ma Kelameili ophiolite belt in the eastern segment (Jian et al., 2005; Tang et al., 2007), and it likely represents relicts of the Junggar back-arc ocean (Dong et al., 2009). The regular arrangement of various magmatic arcs associated with correlated ophiolite belts of the northern Junggar terrane was induced by the southward subduction of the Paleo-Asian oceanic plate beneath the Junggar continent in the early Paleozoic and later intra-oceanic subduction (Xu et al., 2013). The Junggar block is bounded by the Tangbale–Darbute–Kelameili ophiolite belts to the north and Ucharal–Jinghe and Dacaotan fault to the south (Charvet et al., 2001; Dong et al., 2009), and it consists of the Junggar basin, Turpan basin and north Tianshan (Zhang et al., 1984; He et al., 1994). The Central Tianshan Paleozoic magmatic arc is related to the north subduction of the South Tianshan oceanic plate beneath the Yili–Central Tianshan terrane (Chen et al., 1999; Gao et al., 2009; Long et al., 2011; Xiao et al., 2013). The Jiaoluotage tectonic belt that is located between the Central Tianshan range and Junggar block is characterized by the development of a Permian ductile compressive zone (Xu et al., 2003) and bounded by the Dacaotan fault to the north and the Aaikkudug–Shaquanzi thrust fault to the south (Xiao et al., 2004b; Xu and Ma, 2004).

3. Features of new enclaves and gneiss in the Junggar terrane

We recently identified gneiss and magnetite quartzite enclaves in a diorite dike in the Taheir area in the Yemaquan arc, deformed Ordovician conglomerates with gneiss pebbles in the Dazigou in the Junggar block, and gneiss relicts in a granite pluton in the Shuangchagou area in the Jiaoluotage tectonic belts (Fig. 1b). Features of these enclaves, gneiss relicts and their host intrusions, and conglomerates are outlined below.

3.1. Taheir gneiss and magnetite quartzite enclaves

The gneiss and magnetite quartzite enclaves were found in a diorite dike that emplaced in deformed and metamorphosed Ordovician volcanic rocks in the Taheir tectonic window approximately 90 km northwest of the town of Barkol, Xinjiang, China in the Yemaquan arc (Figs. 1b, 2a, b). The gneiss enclaves are elliptic in plan view with lengths ranging from 5 to 9 cm (Fig. 2c). The gneisses consist of oriented hornblende (50 vol.% and 20–300 μm in length), andesine (40 vol.% and 50–120 μm in length) and titanite (8 vol.% and 20–80 μm in diameter) layers with few magnetites (2 vol.%, 20–60 μm in diameter; Fig. 2d, e). The gneiss enclaves are weakly altered and hornblende is partially replaced by chlorite. The magnetite quartzite enclaves are elliptic in plan view with lengths ranging from 5 to 25 cm (Fig. 2f). The magnetite quartzite is characterized by interlayers of hornblende–plagioclase gneisses, magnetite–diopside and diopside–magnetite, and an overprinting of foliation on the bedding structures (Fig. 2g). The magnetite quartzite consists of quartz (85 vol.% and 50–120 μm in diameter) and magnetite (15 vol.% and 20–80 μm in diameter), and are partly replaced by muscovites and titanites (Fig. 2h). The hornblende–plagioclase gneiss interlayers consist of hornblende (25 vol.% and 50–100 μm in length), andesine (45 vol.% and 50–120 μm in length), quartz (15 vol.% and 50–100 μm in diameter) and magnetite (15 vol.% and 50–100 μm in diameter); some andesines and hornblendes are replaced by muscovites and chlorites, respectively (Fig. 2i).

3.2. Dazigou conglomerates

Pebble conglomerates were found at the eastern end of the profile A-A' along a NE-trending valley in the Dazigou area approximately 53 km southeast of the town of Barkol at the north margin of the Junggar block (Figs. 1b, 3a). The pebble conglomerates are present

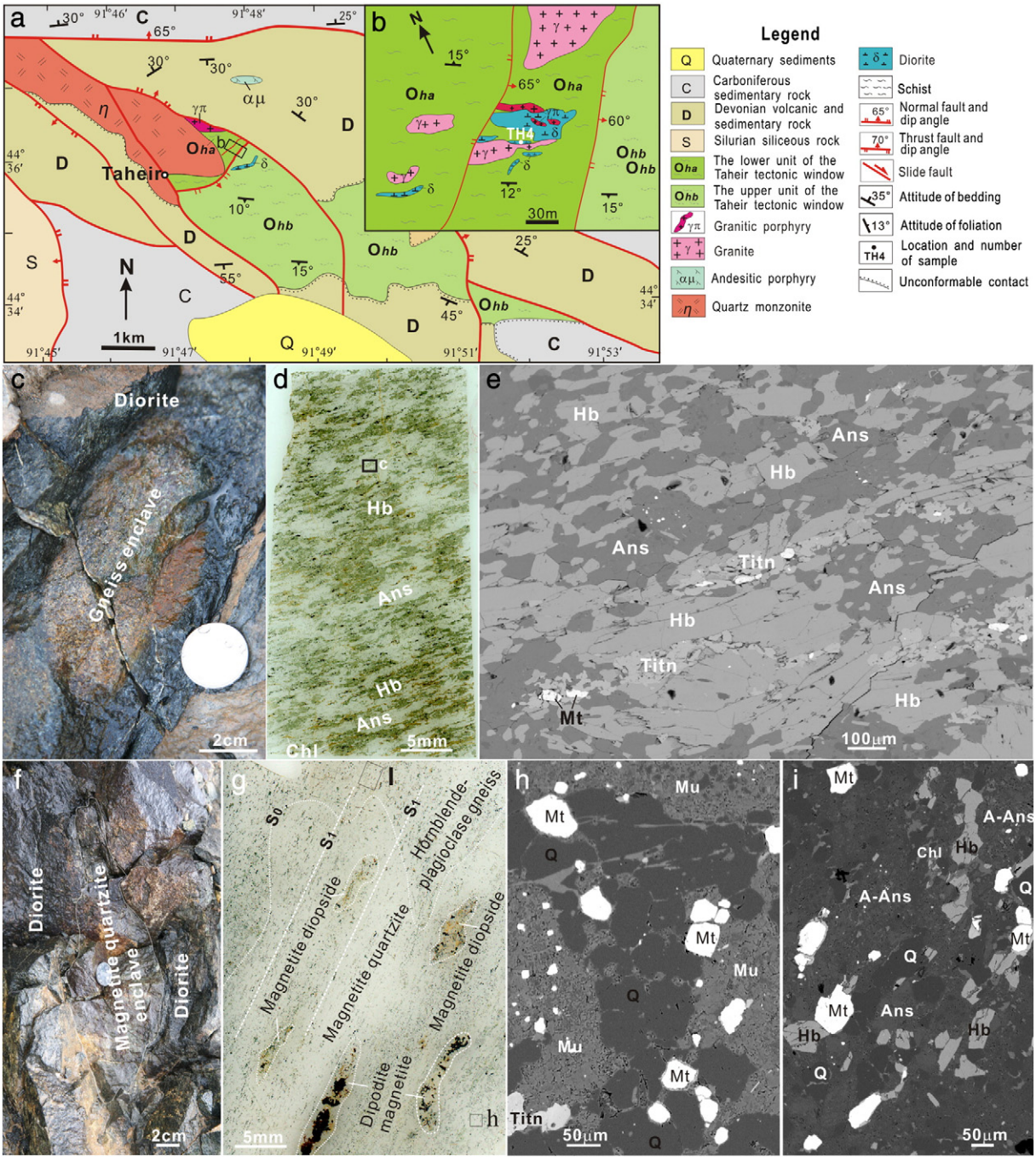

Fig. 2. Geological map (a) with an inserted enlargement (b) of the Taheir area (after Xu et al., 2013), and outcrop (c and f), scanning (d and g) and back scattered electron (e, h and i) images showing the location and macroscopic to microscopic features of enclaves in a diorite dike in the Taheir area. Panels c, d and e are present for a gneiss enclave, whereas panels f, g, h and i for a magnetite quartzite enclave. The location of the Taheir area is shown in Fig. 1b. The surface of the gneiss enclave in panel c was exposed along fractures with brown limonite films. S_0: bedding structure; S_1: foliation structure; A-Ans: altered andesine; Ans: andesine; Chl: chlorite; Hb: hornblende; Mt: magnetite; Mu: muscovite; Q: quartz; Titn: titanite.

at the upper part of the middle Ordovician Wuleigai formation at the center of a NW-trending anticline, and overlain by siltstones and sandstones of the upper Ordovician Miaoergou formation (profile A-A' in Fig. 3). The Wuleigai formation regionally consists of foliated siltstones and mudstones containing *Sowerbyella* sp., *Onniell* sp., *Orthambonites* sp., *Dalmanellids*, *Cryptothris* sp. and *Aegiromena* sp. in the lower part, foliated limestone containing *Howellites* sp., *Sperorthis* sp., *Hesperorthis* sp., *Atrypa* sp., *Leptelloidea* sp., and *Resserella* sp. in the middle part, and flattened conglomerates, foliated quartz sandstones and andesites in the upper part (XJBGMR, Xinjiang Bureau of Geology (2009). The conglomerates in the Dazigou area contain quartzite, siltstone, sandstone, tuff, granite, granite porphyry, granitic mylonite, gneiss and amphibolite pebbles within the quartz matrix (Fig. 3b–e). Most of the quartzite pebbles are well rounded, whereas some siltstone, granitic mylonite, gneiss and amphibolite pebbles are sub-angular to sub-rounded (Fig. 3b). The pebble conglomerates are intensively flattened and foliated. The matrix quartzes and quartzites are stretched with evident wavy extinctions (Fig. 3c). Foliations exhibited by oriented sericite zones are well developed in some siltstone, sandstone, tuff and granite porphyry pebbles (Fig. 3d). Some of the granitic mylonites exhibit two-stage deformation structures, and the rotating porphyroclasts and folded quartz flowing zones are overprinted by oriented sericite zones (Fig. 3e).

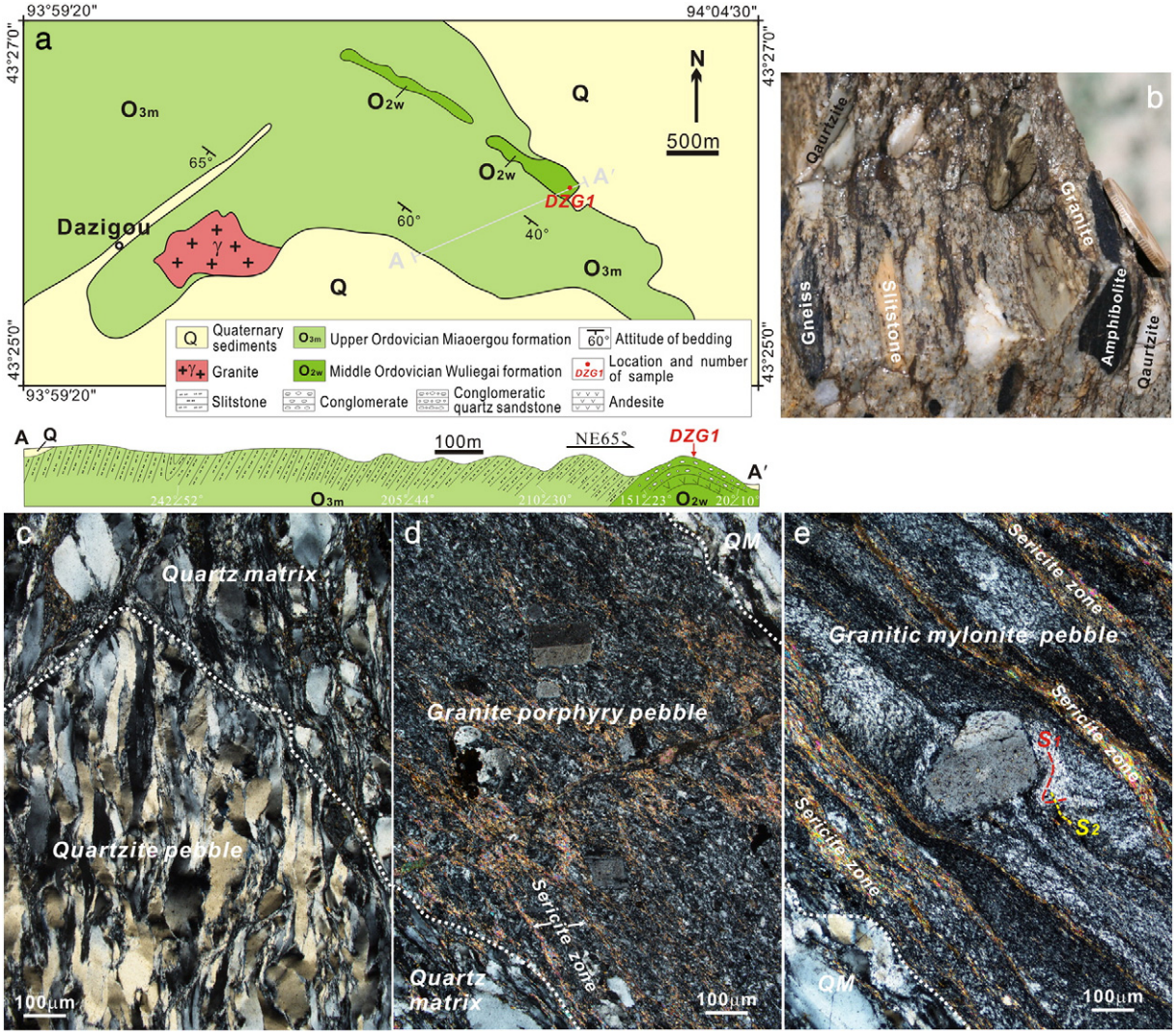

Fig. 3. Geological map of the Dazigou area (a) (revised from XJBGMR, Xinjiang Bureau of Geology (2009) with a profile A-A′ and sample (b) and crossed polarized (c, d and e) images of deformed pebble conglomerates. The diameter of the coin in panel b is 2 cm. The location of the Dazigou area is shown in Fig. 1b. The white dotted lines in panels c, d and e show the surface boundary of the pebbles. S_1: foliation structure formed in the first deformation stage; S_2: foliation structure formed in the second deformation stage; QM: quartz matrix.

3.3. Shuangchagou gneiss

Relicts of folded gneisses are present in a syn-tectonic granite pluton emplaced into the Jiaoluotage ductile compressional zone in the Shuangchagou area approximately 80 km southeast of Hami City (Figs. 1b, 4a; Xu et al., 2003). The gneisses consist of biotite–plagioclase, quartz–biotite and mica gneisses. The mica gneisses have irregularly curved boundaries that cut through the biotite–plagioclase and quartz–biotite gneisses as intrusions (Fig. 4b), and they are characterized by layered structures (Fig. 3c) and consist of biotite (25 vol.% and 100–800 μm in length), muscovite (15 vol.% and 200–700 μm in length), hornblende (5 vol.% and 50–150 μm in diameter), diopside (2 vol.% and 80–160 μm in diameter) and andesine (52 vol.% and 100–300 μm in diameter) (Fig. 4d, e).

4. Sample selection and analytical techniques

An 8.6 × 4.4 cm gneiss enclave (sample TH4-1), 25 × 8 cm magnetite quartzite enclave (sample TH4-2) and their host diorite (sample TH4-6, approximately 20 kg) from the Taheir area, a mica gneiss (sample SCG3, approximately 15 kg) and a host granite (sample SCG2, approximately 5 kg) from the Shuangchagou area, and a conglomerate (sample DZ1, approximately 25 kg) from the Dazigou area were selected for the zircon U–Pb–Hf isotope and geochemical analysis. All analyses were conducted at the Institute of Geology and Geophysics, Chinese Academy of Sciences (IGGCAS).

For geochemical analyses, hand specimens were crushed in a tungsten carbide swing mill, sieved, ultrasonically cleaned several times in deionized water and then ground in an agate mortar. Rock powders (~1.2 g) were then dissolved with $Li_2B_4O_7$ (6 g) in a TR-1000S automatic bead fusion furnace at 1100 °C for 10 min. Major element abundances (wt.%) were determined on whole-rock powder pellets by X-ray fluorescence (XRF) using an XRF-1500 sequential spectrometer. Analytical uncertainties are 1 to 3% for major elements. Loss on ignition was obtained by weighing after 1 h of calcinations at 1100 °C. Major element data from the analyzed samples of the Junggar terrane are summarized in Supplementary Table 1.

Zircon grains were separated by using conventional heavy fraction and magnetic techniques. Representative zircon grains, together with zircon standard Qinghu (159.5 Ma, Li et al., 2013) and standard 91500 (1065 Ma, Wiedenbeck et al., 1995), were mounted in epoxy mounts which were then polished to a section the crystals in half for analysis. More than one thousand zircon grains were separated from the diorite, granite and mica gneiss (samples TH4-6, SCG2 and SCG3, respectively), and about two hundred of them were mounted in a row. Less than two hundred zircon grains were separated from the gneiss and magnetite

Fig. 4. Remote sensing (a), outcrop (b), scanning (c) and microscopic (d and e) images showing the location and macroscopic to microscopic features of the gneiss relicts within a granite emplaced in the Jiaoluotage tectonic belt in the Shuangchagou area. Images d and e are plane and crossed polarized images, respectively. The location of the Shuangchagou area is shown in Fig. 1b. Ans: andesine; Bi: biotite; BP: biotite-plagioclase; C: Carboniferous strata; Di: diopside; Hb: hornblende; Mu: muscovite; QB: quartz–biotite. The dashed lines in panel a show the attitude of the foliations.

quartzite enclaves (samples TH4-1 and TH4-2), and all of them were mounted in a row. The zircon grains separated from the conglomerate sample (DZG1) were divided into five populations on basis of crystal color and morphology, and correspondingly mounted in five rows. All mounted zircons were documented with transmitted and reflected light micrographs as well as cathodoluminescence (CL) images to reveal their internal structures, and the mount was vacuum-coated with high-purity gold prior to secondary ion mass spectrometry (SIMS) analysis. Following the CL and other imaging, the samples were vacuum-coated with high-purity gold.

Measurements of U, Th and Pb were conducted by using the Cameca IMS-1280 SIMS. U–Th–Pb ratios and absolute abundances were determined relative to the standard zircon 91500 (Wiedenbeck et al., 1995), analyses of which were interspersed with those of unknown grains, using operating and data processing procedures similar to those described by X.H. Li et al. (2009b). A long-term uncertainty of 1.5% (1 RSD) for $^{206}Pb/^{238}U$ measurements of the standard zircons was propagated to the unknowns (Li et al., 2010), despite that the measured $^{206}Pb/^{238}U$ error in a specific session is generally around 1% (1 RSD) or less. Measured compositions were corrected for common Pb by using non-radiogenic ^{204}Pb. Corrections are sufficiently small to be insensitive to the choice of common Pb composition, and an average of present-day crustal composition (Stacey and Kramers, 1975) is used for the common Pb assuming that the common Pb is largely surface contamination introduced during sample preparation. Uncertainties on individual analyses in data tables are reported at a 1 σ level; mean ages for pooled U/Pb (and Pb/Pb) analyses are quoted with 95% confidence interval. Data reduction was carried out by using the Isoplot/Ex v. 2.49 programs (Ludwig, 2001).

In order to monitor the external uncertainties of SIMS U–Pb measurements calibrated against 91500 standard, Qinghu zircon standard was alternately analyzed as an unknown together with the unknown zircons that were mounted in Mounts A1629 (containing samples TH4-1, TH4-2, TH4-6 and 10TK01), A2131 (containing samples SCG2,3), and A2132 (containing sample DZG1) during the course of this study. A total of 54 measurements were conducted on Qinghu (Supplementary Table 2), and the Concordia Age (Ludwig, 2001) of 159.24 ± 0.50 Ma (MSWD = 0.52), 159.0 ± 0.62 Ma (MSWD = 0.70), and 159.8 ± 0.62 Ma (MSWD = 0.021) was obtained for Qinghu in Mount A1629, A2131 and A2132, respectively. These three measured ages give a mean of 159.33 ± 0.53 Ma (2SD), which is identical within error with the recommended value of 159.5 ± 0.2 Ma (Li et al., 2013), and an external uncertainty of our SIMS U–Pb age determination is ca. ±0.3% (2SD).

In situ zircon Lu–Hf isotopic analyses were carried out by using a Neptune MC–ICPMS with an ArF excimer laser ablation system. Hf isotopic analyses were obtained on the same zircon grains that were previously analyzed for U–Pb isotopes, with ablation pits of 40 μm in diameter, and a laser repetition rate of 10 Hz with 100 mJ were used. Details of the technique are described by Xu et al. (2004), Wu et al. (2006) and Li et al. (2010). During analyses, the $^{176}Hf/^{177}Hf$ and $^{176}Lu/^{177}Hf$ ratios of standard zircon (91500) were 0.282294 ± 15 ($2\sigma_n$, n = 20) and 0.00031, similar to the commonly accepted $^{176}Hf/^{177}Hf$ ratio of 0.282284 ± 3 (1σ) measured by using the solution method (Goolaerts et al., 2004; Woodhead et al., 2004).

5. Analytical results

5.1. Whole rock geochemistry

The diorite TH4-6 contains SiO_2 at 52.65 wt.%, Al_2O_3 at 14.42 wt.%, Fe_2O_3 at 12.11 wt.%, MgO at 4.51 wt.%, CaO at 8.59 wt.%, Na_2O at 2.70 wt.%, and K_2O at 1.28 wt.%. The gneiss enclave TH4-1 has similar geochemical signatures with its host diorite (sample TH4-6), with SiO_2 at 53.37 wt.%, Al_2O_3 at 15.04 wt.%, Fe_2O_3 at 11.60 wt.%, MgO at 4.68 wt.%, CaO at 8.69 wt.%, Na_2O at 2.06 wt.%, and K_2O at 1.35 wt.%.

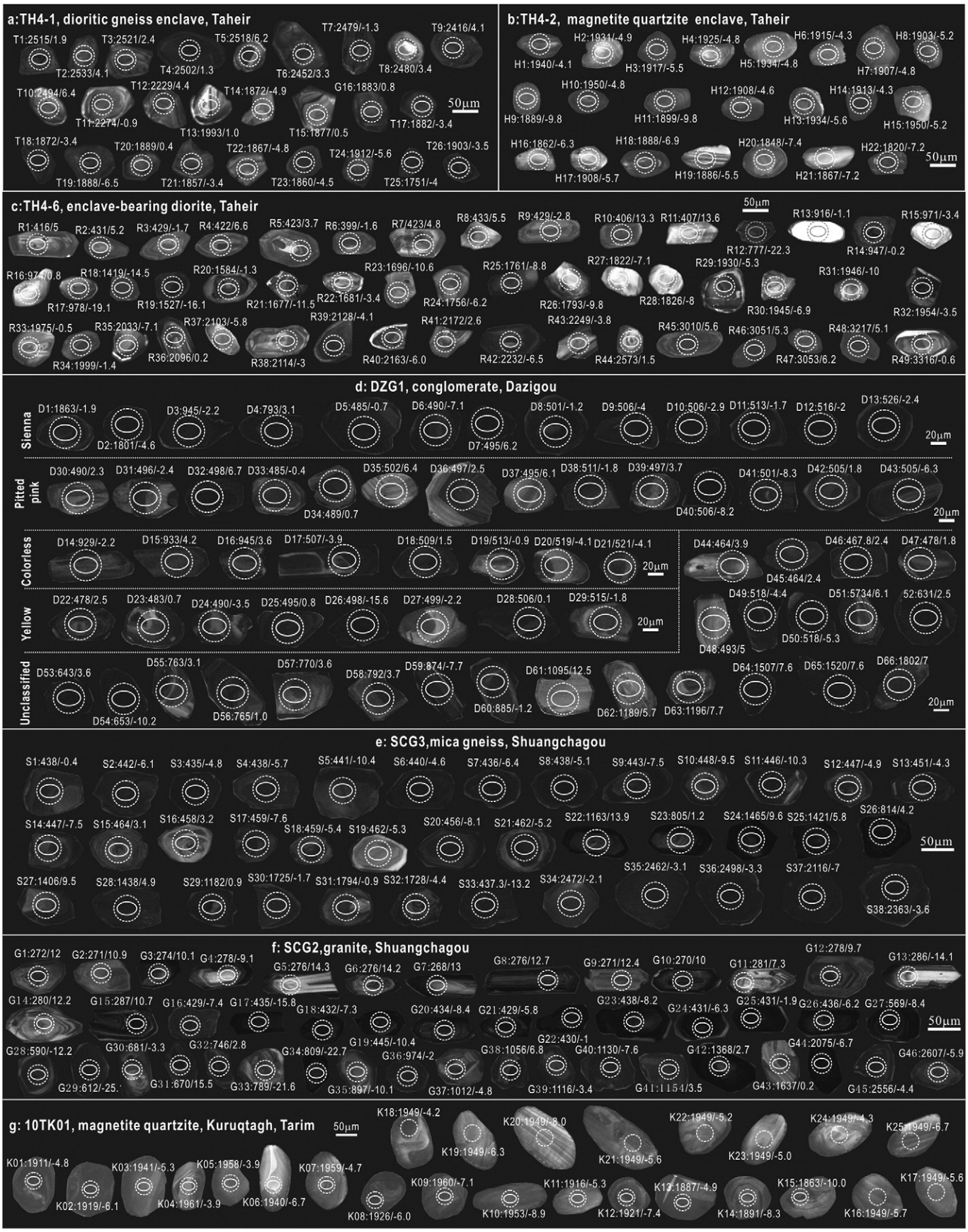

Fig. 5. Cathodoluminescence (CL) images of representative zircon grains selected for the SIMS U–Pb dating and LA–ICPMS Hf isotope analysis in this study. The white solid ellipses show the location and size of the laser ablation for the SIMS U–Pb dating, whereas the white dotted circles show the LA–ICPMS Hf isotope analysis. The grain and spot number, $^{206}Pb/^{238}U$ age (≤800 Ma) or $^{206}Pb/^{207}Pb$ age (>800 Ma) value, and initial $\varepsilon Hf_{(t)}$ value of zircon were labeled aside the white solid ellipsis and dotted circle.

Although the geochemistry of the gneiss enclave and the country rocks is similar, the gneiss enclave has banding structure with sharp boundary to its host diorite, and the diorite has distinct granitic structure. The magnetite quartzite enclave TH4-2 has high amounts of SiO_2 (80.86 wt.%) and Fe_2O_3 (9.68 wt.%), and the conglomerate DZG1 has high amounts of SiO_2 (82.65 wt.%) and Al_2O_3 (13.22 wt.%). The mica gneiss SCG3 contains SiO_2 at 64.2 wt.%, Al_2O_3 at 15.87 wt.%, Fe_2O_3 at 6.77 wt.%, MgO at 3.08 wt.%, CaO at 1.05 wt.%, Na_2O at 1.3 wt.%, and K_2O at 4.88 wt.%. The granite SCG2 contains SiO_2 at 73.85 wt.%, Al_2O_3 at 14.3 wt.%, Fe_2O_3 at 1.84 wt.%, MgO at 0.49 wt.%, CaO at 2.48 wt.%, Na_2O at 3.84 wt.%, and K_2O at 2.16 wt.%.

5.2. Zircon features, U–Pb ages and Lu–Hf isotopes

The CL images of the representative zircons selected for U–Pb dating and Hf analyses are shown in Fig. 5. The SIMS zircon U–Th–Pb isotopic data are present in Supplementary Table 3 and illustrated in Figs. 6–8. The LA-ICPMS zircon Hf isotopic data are reported in Supplementary Table 4. The initial $\varepsilon Hf_{(t)}$ values and corresponding Hf-depleted mantle model ages (T_{DM}) have been calculated at their corresponding zircon $^{206}Pb/^{238}U$ age (≤800 Ma) or $^{206}Pb/^{207}Pb$ age (>800 Ma; Dhuime et al., 2012; Jiang et al., 2012). The single-stage model ages (T_{DM1}) are calculated by referencing the depleted mantle with a present-day $^{176}Hf/^{177}Hf$ ratio of 0.28325 and $^{176}Lu/^{177}Hf = 0.0384$ (Vervoort and Blichert-Toft, 1996), and the two-stage model ages (T_{DM2}) are calculated by assuming an $^{176}Lu/^{177}Hf$ ratio of 0.009 for the average upper continental crust (Amelin et al., 1999). The crustal model age (T_{DMC}) assumes that its parental magma was produced from an average continental crust ($^{176}Lu/^{177}Hf = 0.015$) that was originally derived from the depleted mantle (Griffin et al., 2004).

5.2.1. Taheir gneiss and magnetite quartzite enclaves and diorite

Zircons from the gneiss enclave TH4-1 are relatively transparent and pink, have a gray color in the CL images and are equant to short prismatic with lengths ranging from 50 to 120 μm and length/width ratios of 1:1 to 2:1 (Fig. 5a). Most of the zircons are euhedral to subhedral with clear or weak oscillatory zoning to no internal zoning, whereas a small amount the zircons are anhedral without zoning. The zircons can be divided into two types: magmatic zircons with clear or weak oscillatory zoning and metamorphic recrystallized zircons with blurred or no internal zoning. The magmatic zircons contain 63–2285 ppm U, 28–1013 ppm Th and 37–412 ppm Pb with Th/U ratios in the range of 0.031–1.471, $^{207}Pb/^{206}Pb$ ages ranging from 1903 ± 6.7 Ma to 2533.3 ± 4.7 Ma, $^{206}Pb/^{238}U$ ages ranging from 917.9 ± 14.7 Ma to 2537.3 ± 31.6 Ma, $^{176}Hf/^{177}Hf$ values from 0.281165 to 0.281486, $\varepsilon_{Hf\ (t)}$ values from −3.5 to +6.4, and variable T_{DM1} (2411–2839 Ma), T_{DMC} (2534–3090 Ma) and T_{DM2} (2522–3063 Ma) for 13 analyzed grains (Grains T1–T12, T26). Eleven points for 11 grains of the magmatic zircons define the discordia line BA, which has an upper intercept age of 2517 ± 23 Ma and an imprecise lower intercept age of 524 ± 140 Ma (MSWD = 13); the upper intercept age (2517 ± 23 Ma) is consistent with the concordia age (2522.5 ± 16 Ma, MSWD = 2.4) of three of the 11 points (Fig. 6a), whereas the remaining two points for two grains of magmatic zircons are on the line BC, which has an upper intercept age of 2573 ± 52 Ma

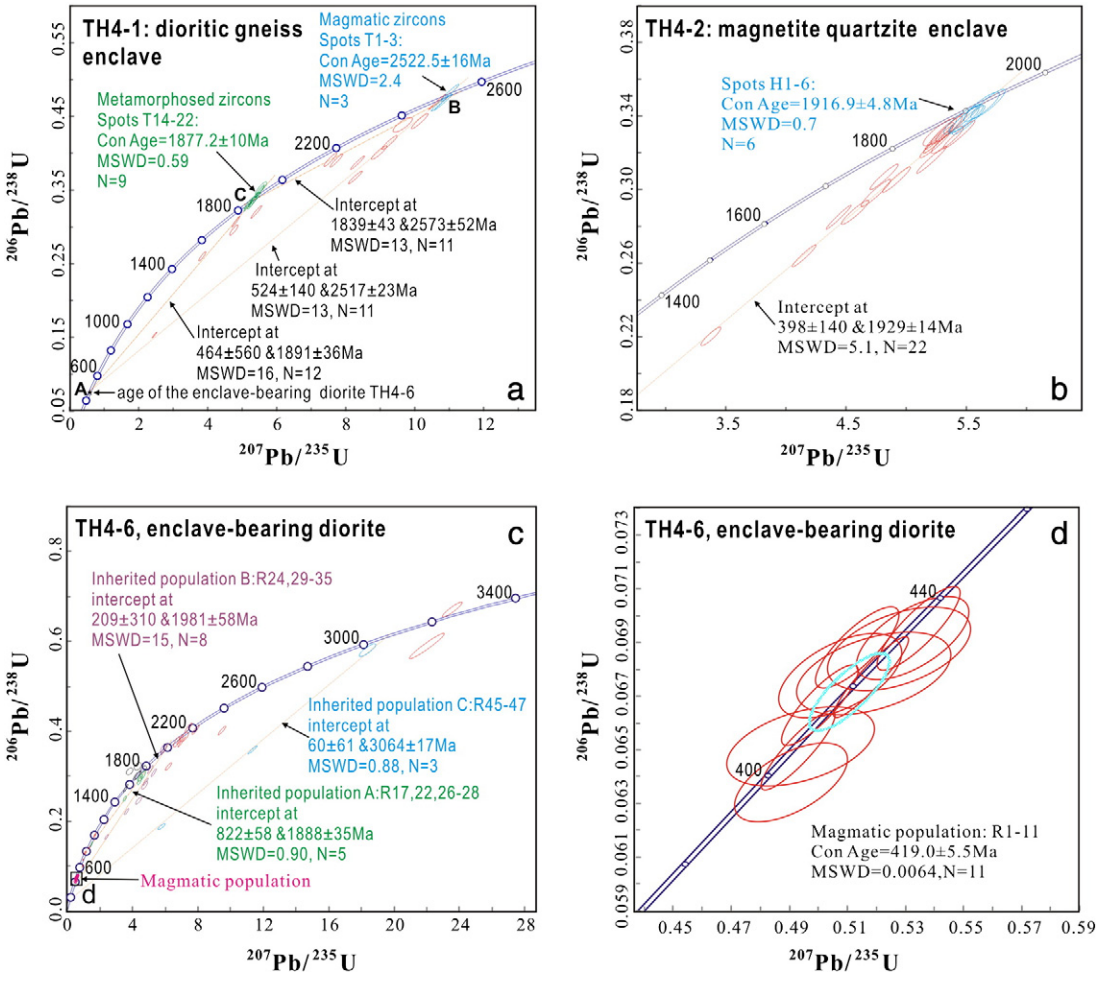

Fig. 6. Zircon SIMS U–Pb concordia age plots of enclaves of gneiss and magnetite quartzite interlayered with hornblende–plagioclase gneiss layers and diorite from the Taheir area.

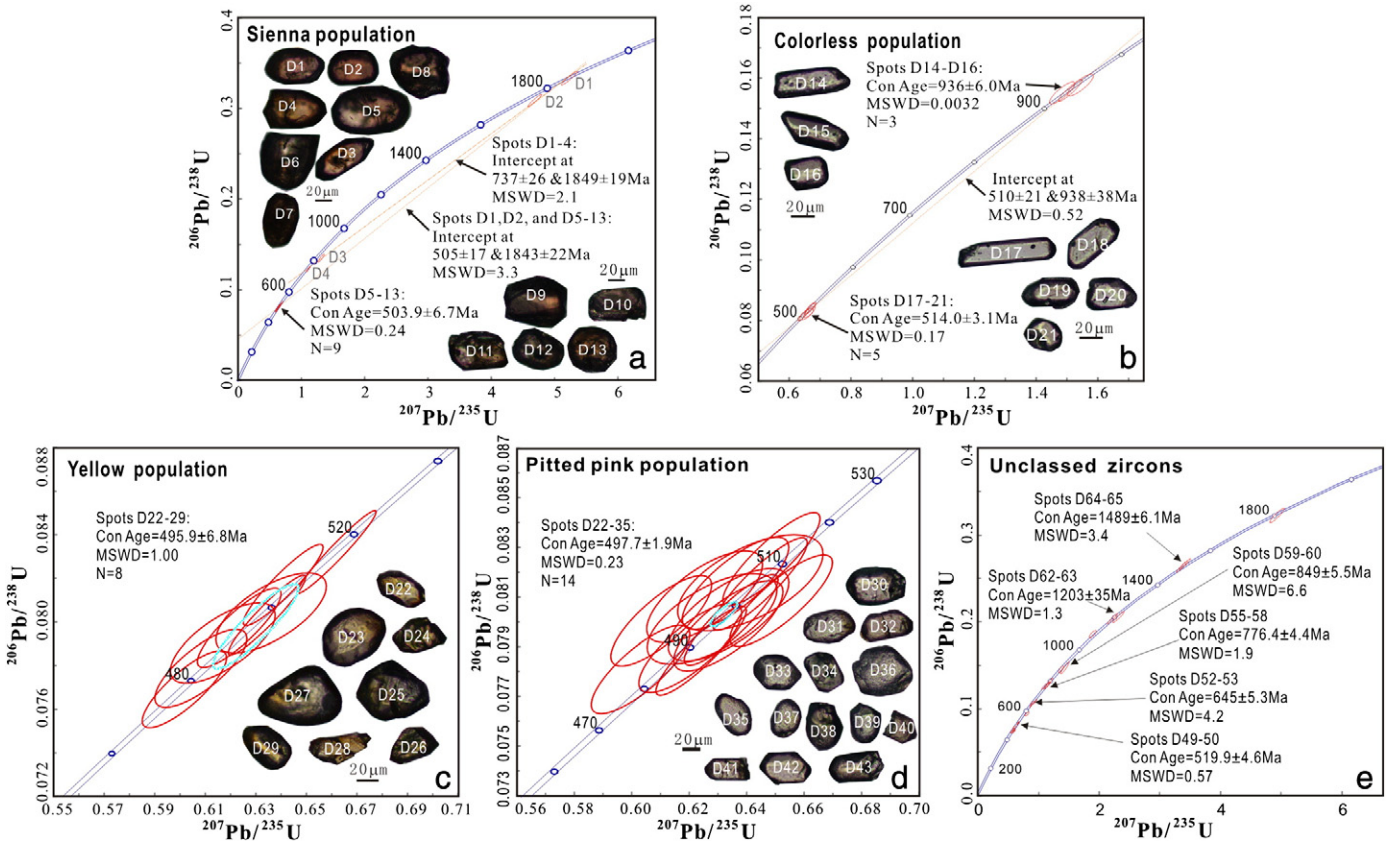

Fig. 7. Zircon SIMS U–Pb concordia age plots of the conglomerate DZG1 from the Dazigou area. Morphological images of representative zircons of the sienna, colorless, yellow and pink populations are inserted into their concordia age plot diagrams.

and a lower intercept age of 1839 ± 43 Ma (MSWD = 13). The metamorphic recrystallized zircons have 176–2799 ppm U, 3–679 ppm Th and 72–2493 ppm Pb with Th/U ratios in the range of 0.008–0.443, $^{207}Pb/^{206}Pb$ ages ranging from 1750.5 ± 10.8 Ma to 1992.8 ± 10.3 Ma, $^{206}Pb/^{238}U$ ages ranging from 1492.3 ± 21.1 Ma to 1944.6 ± 25.3 Ma, $^{176}Hf/^{177}Hf$ values from 0.281140 to 0.281607, $\varepsilon_{Hf\ (t)}$ values from −6.5 to +0.8, and variable T_{DM1} (2255–2529 Ma), T_{DMC} (2499–2962 Ma) and T_{DM2} (2479–2929 Ma) for 13 analyzed grains (Grains T13–T25). The 13 points for 13 grains of the metamorphic recrystallized zircons define the discordia line CA, which has an upper intercept age of 1891 ± 36 Ma and an imprecise lower intercept age of 464 ± 560 Ma (MSWD = 16); the upper intercept age (1891 ± 36 Ma) is consistent with the concordia age (1877.2 ± 10 Ma, MSWD = 0.59) of nine of the 13 points.

Zircons from the magnetite quartzite that is interlayered with hornblende–plagioclase gneiss layers (enclave TH4-2) are relatively transparent and purple, have a gray color in the CL images and are equant to short prismatic with lengths ranging from 60 to 115 μm and length/width ratios of 1:1 to 2.4:1. Most of the zircons are subhedral to anhedral morphology with blurred or weak zoning, and a small amount of the zircons are sub-rounded with thin rims (Fig. 5b). These zircons have 130–1117 ppm U, 32–401 ppm Th and 58–365 ppm Pb with Th/U ratios in the range of 0.108–0.630, $^{207}Pb/^{206}Pb$ ages ranging from 189.9 ± 11.9 Ma to 1950.1 ± 7.7 Ma (Supplementary Table 3), $^{176}Hf/^{177}Hf$ values from 0.281319 to 0.281485, $\varepsilon_{Hf\ (t)}$ values from −9.8 to −4.0, and similar T_{DM1} (2451–2668 Ma), T_{DMC} (2817–3128 Ma) and T_{DM2} (2788–3144 Ma) for 22 analyzed grains (Supplementary Table 4). These zircons define a discordia line with an upper intercept age of 1929 ± 14 Ma and a lower intercept age of 398 ± 140 Ma (MSWD = 13), and they have an upper intercept age (1929 ± 14 Ma) that is consistent with the concordia age (1916.9 ± 4.8 Ma, MSWD = 0.7) of seven of the 22 points (Fig. 6b).

Zircons from the diorite TH4-6 are classified into magmatic (co-magmatically grown) zircons and inherited zircons (residual from source or ambient rock). The magmatic zircons are euhedral, transparent and colorless, have gray color and zoning in the CL images and are short to long prismatic with lengths ranging from 70 to 140 μm and length/width ratios of 1.5:1 to 3.5:1 (Fig. 5c). The magmatic zircons have 178–2803 ppm U, 17–13,561 ppm Th and 14–420 ppm Pb with Th/U ratios in the range of 0.059–4.838, $^{206}Pb/^{238}U$ ages ranging from 398.6 ± 5.8 Ma to 433.3 ± 6.3 Ma with a concordia age of 419.0 ± 5.5 Ma (MSWD = 0.0064; Supplementary Table 3, Fig. 6c,d), $^{176}Hf/^{177}Hf$ values from 0.282450 to 0.282964, $\varepsilon_{Hf\ (t)}$ values from −2.8 to +13.6, and variable T_{DM1} (501–1187 Ma), T_{DMC} (531–1595 Ma) and T_{DM2} (530–1590 Ma) for 11 analyzed grains (Supplementary Table 4). The inherited zircons from the diorite TH4-6 are complex with various color that ranges from colorless to yellow to pale pink; most of them are euhedral to subhedral with clear or weak zoning and equant to long prismatic with lengths ranging from 60 to 140 μm and length/width ratios of 1:1 to 3.0:1 (Fig. 5c). The inherited zircons have 37–2307 ppm U, 32–1518 ppm Th and 12–564 ppm Pb with Th/U ratios in the range of 0.105–2.188, $^{207}Pb/^{206}Pb$ ages ranging from 776.9 ± 34.4 Ma to 3316.3 ± 12 Ma (Supplementary Table 3), $^{176}Hf/^{177}Hf$ values from 0.280669 to 0.282208, $\varepsilon_{Hf\ (t)}$ values from −22.3 to +6.2, and variable T_{DM1} (1473-3532 Ma), T_{DMC} (1792–3688 Ma) and T_{DM2} (1780–3666 Ma) for 39 analyzed grains (Supplementary Table 4). Among these 39 analyzed inherited grains, four zircon couples and three zircon populations with similar morphology and internal textures were identified. Grains R15 and R16 have a bright gray CL color, weak zoning, and concordia ages of 984 ± 7.5 Ma (MSWD = 1.3); anhedral grains R21 and R23 have clear zoning, a gray color in the CL images, and concordia ages of 1685 ± 9.5 Ma (MSWD = 0.49); subhedral grains R37 and R38 have weak zoning, a gray color in the CL images and

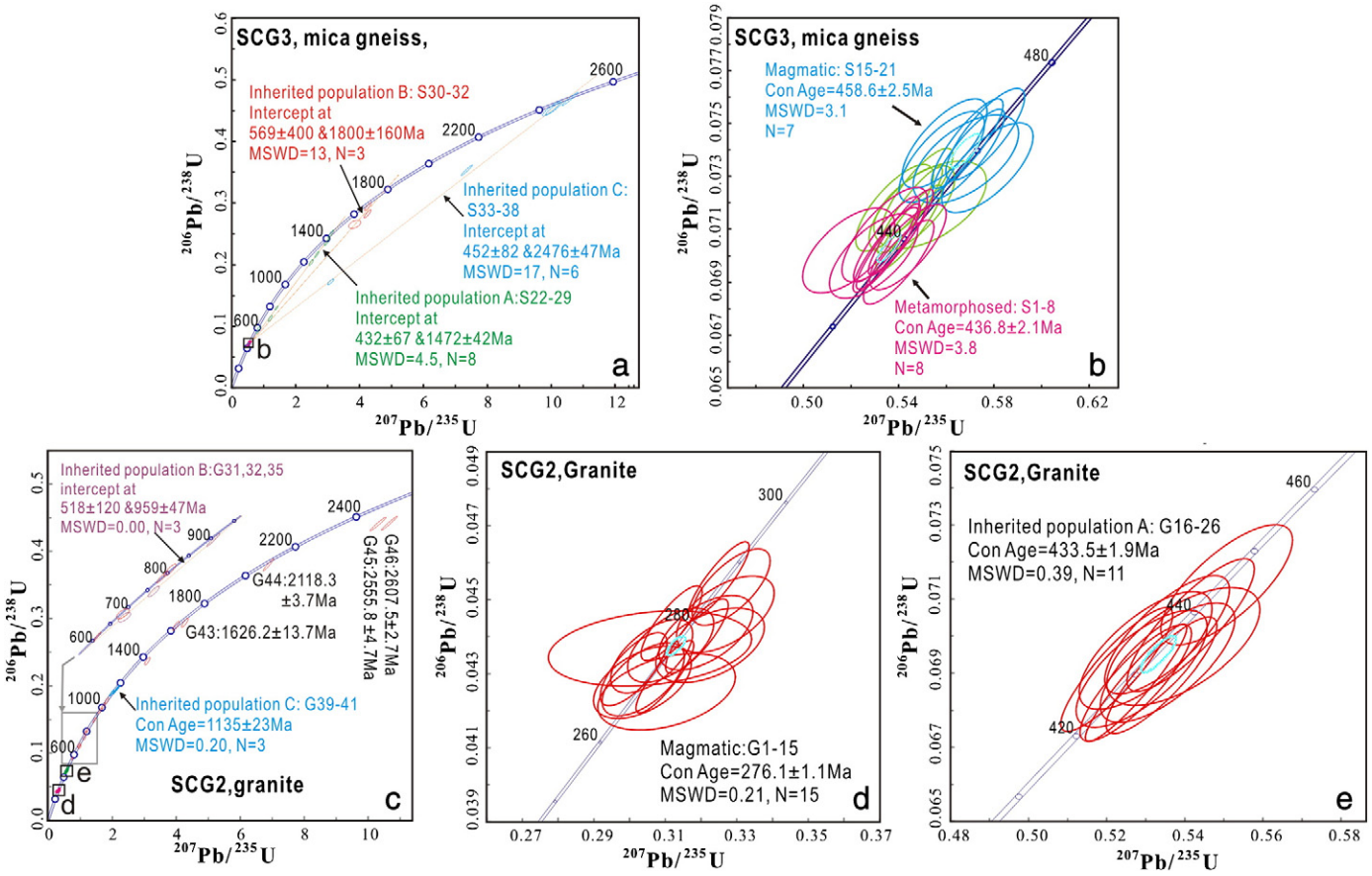

Fig. 8. Zircon SIMS U–Pb concordia age plots of the mica gneiss SCG3 and granite SCG2 from the Shuangchagou area.

concordia ages of 2015 ± 9.5 Ma (MSWD = 4.1); and grains R39 and R40 have clear sub-rounded rim, clear zoning, gray color in the CL images, and 2133 ± 35 Ma (MSWD = 0.86). Grains R17, R22 and R26–28 (population A) have a sub-rounded morphology, weak or no zoning, a gray color in the CL images, and yield a discordia line with an upper intercept age of 1888 ± 35 Ma (MSWD = 0.9); grains R24 and R29–35 (population B) have an equant and subhedral morphology, weak zoning, and gray color in the CL images that defines a discordia line with an upper intercept age of 1981 ± 58 Ma (MSWD = 15); grains R45–47 (population C) have an elliptic morphology, weak zoning and gray color in the CL images that defines a discordia line with an upper intercept age of 3064 ± 17 Ma (MSWD = 0.88; Fig. 6c), which is similar to the Hf model ages, i.e., $T_{DM1} \approx T_{DMC} \approx T_{DM2} \approx$ ~3.04 Ga for grain R45, $T_{DM1} \approx T_{DMC} \approx T_{DM2} \approx$ ~3.09 Ga for grain R46, and $T_{DM1} \approx T_{DMC} \approx T_{DM2} \approx$ ~3.04 Ga for grain R45, $T_{DM1} = T_{DMC} = T_{DM2} = 3.05$ Ga for grain R47. Moreover, the four grains R12, R19, R25 and R48 with euhedral to subhedral morphology and weak to blurred zoning and a gray color in the CL images that plots on or near the crust evolution line with a $^{206}Pb/^{238}U$ age of 781.9 ± 11.1 Ma and a $^{207}Pb/^{206}Pb$ ages of 1552.6 ± 10.7 Ma, 1760.6 ± 33.4 Ma and 3216.7 ± 11.1 Ma, respectively.

5.2.2. Dazigou conglomerate

On the basis of zircon color, four different zircon populations were identified from the zircon grains separated from the conglomerate sample (DZG1): sienna, colorless, yellow and pink zircon population (Fig. 7a–d).

The sienna zircons are euhedral to subhedral, have a dark gray color and weak or no zoning in the CL images and are equant to short prismatic with lengths ranging from 45 to 110 μm and length/width ratios of 1:1 to 2:1 (Fig. 5d); these zircons have 562–4574 ppm U, 72–1354 ppm Th and 53–548 ppm Pb with Th/U ratios in the range of 0.047–0.702, $^{206}Pb/^{238}U$ ages ranging from 490.2 ± 7.1 Ma to 1855 ± 24.2 Ma, $^{207}Pb/^{206}Pb$ ages ranging from 488.3 ± 20 Ma to 1862.5 ± 7.4 Ma (Supplementary Table 3), $^{176}Hf/^{177}Hf$ values from 0.281525 to 0.282646, $\varepsilon_{Hf\ (t)}$ values from −7.1 to +6.2, and variable T_{DM1} (853–2386 Ma), T_{DMC} (1078–2779 Ma) and T_{DM2} (1074–2750 Ma) for 13 analyzed grains (spots D1–13). Among these 13 analyzed grains, grain D1 with a euhedral morphology and weak zonation has a $^{206}Pb/^{238}U$ age of 1855 ± 24.2 Ma, $^{207}Pb/^{206}Pb$ age of 1862.5 ± 7.4 Ma, T_{DM1} of 2341 Ma, T_{DMC} of 2653 Ma and T_{DM2} of 2628 Ma; grains D5–13 have a weak resorbed surfaces, no zoning internal texture, a concordia age of 503.9 ± 6.7 Ma (MSWD = 0.24) and similar T_{DM1} (853–1386 Ma), T_{DMC} (1078–1920 Ma) and T_{DM2} (1074–1914 Ma); grains D1–4 define a discordia line with an upper intercept age of 1849 ± 19 Ma and lower intercept age of 737 ± 26 Ma (MSWD = 2.1); grains D1–2 and D5–13 yield a discordia line with an upper intercept age of 1843 ± 22 Ma and lower intercept age of 505 ± 17 Ma (MSWD = 3.3; Fig. 7a).

The colorless zircons are euhedral, have a gray color and weak zonation in the CL images and are short to long prismatic with lengths ranging from 80 to 150 μm and length/width ratios of 1.5:1 to 3:1 (Fig. 5d). These zircons have 249–919 ppm U, 54–330 ppm Th and 25–108 ppm Pb with Th/U ratios in the range of 0.132–1.005, $^{206}Pb/^{238}U$ ages ranging from 507.1 ± 7.3 Ma to 944.9 ± 13.3 Ma, $^{207}Pb/^{206}Pb$ ages ranging from 502.6 ± 16.6 Ma to 955.9 ± 19.7 Ma (Supplementary Table 3), $^{176}Hf/^{177}Hf$ values from 0.282167 to 0.282506, $\varepsilon_{Hf\ (t)}$ values from −4.1 to +4.3, and variable T_{DM1} (1051–1578 Ma), T_{DMC} (1387–1959 Ma) and T_{DM2} (1381–1945 Ma) for 8 analyzed grains (spots D14–21). All of the 8 analyzed grains define a discordia line with an upper intercept age of 938 ± 38 Ma and lower intercept age of 510 ± 21 Ma (MSWD = 0.52). Among these 8 analyzed grains, grains D14–16 have a euhedral morphology, weak zonation, and

a concordia age of 938 ± 6.0 Ma (MSWD = 0.0032), whereas grains D17–21 have a weak resorbed surface and a concordia age of 514.0 ± 3.1 Ma (MSWD = 0.17; Fig. 7b).

The yellow zircons are subhedral to anhedral, have a gray color and weak zonation in the CL images, and are short prismatic with lengths ranging from 80 to 120 μm and length/width ratios of 1.5:1 to 2.5:1 (Fig. 5d), and have 161–4887 ppm U, 70–1988 ppm Th and 16–481 ppm Pb with Th/U ratios in the range of 0.223–0.452, $^{206}Pb/^{238}U$ ages ranging from 477.6 ± 6.9 Ma to 515.2 ± 7.4 Ma with a concordia age of 495.9 ± 6.8 Ma (MSWD = 1.0; Fig. 7c), $^{176}Hf/^{177}Hf$ values from 0.281041 to 0.282554, $\varepsilon_{Hf\ (t)}$ values from −15.6 to +2.5, and variable T_{DM1} (985–1750 Ma), T_{DMC} (1298–2457 Ma) and T_{DM2} (1294–2452 Ma) for 8 analyzed grains (spots D22–29).

The pink zircons are characterized by a pitted surface and have a subhedral to sub-rounded morphology, a gray color and clear or weak zonation in the CL images, and are equant to short prismatic with lengths ranging from 60 to 120 μm and length/width ratios of 1.2:1 to 2.5:1 (Fig. 5d). These zircons have 192–2832 ppm U, 87–990 ppm Th and 19–269 ppm Pb with Th/U ratios in the range of 0.335–0.765, $^{206}Pb/^{238}U$ ages ranging from 484.7 ± 7.0 Ma to 511.2 ± 7.4 Ma with a concordia age of 497.7 ± 1.9 Ma (MSWD = 0.23; Fig. 7d), $^{176}Hf/^{177}Hf$ values from 0.282234 to 0.282657, $\varepsilon_{Hf\ (t)}$ values from −8.3 to +6.7, and variable T_{DM1} (832–1429 Ma), T_{DMC} (1045–2001 Ma) and T_{DM2} (1041–1995 Ma) for 14 analyzed grains (spots D30–43).

Except for the above four distinct zircon populations, 23 unclassified grains (grains D44–66) were analyzed. The 23 grains are euhedral to subhedral, have gray color and clear or weak zonation in the CL images, and are equant to short prismatic with lengths ranging from 60 to 130 μm and length/width ratios of 1.2:1 to 2.5:1 (Fig. 5d). They have 160–7046 ppm U, 41–1689 ppm Th and 16–824 ppm Pb with Th/U ratios in the range of 0.034–1.057, plots on or near the concordia line with $^{206}Pb/^{238}U$ ages ranging from 463.7 ± 6.7 Ma to 1801.9 ± 23.7 Ma, $^{207}Pb/^{206}Pb$ ages ranging from 416.6 ± 30 Ma to 1818.3 ± 10.1 Ma, $^{176}Hf/^{177}Hf$ values from 0.281848 to 0.282614, $\varepsilon_{Hf\ (t)}$ values from −10.2 to +12.5, and variable T_{DM1} (895–1944 Ma), T_{DMC} (1149–2029 Ma) and T_{DM2} (1144–2022 Ma). Among these 23 analyzed grains, five couple zircons and a four-zircon population with similar morphology and internal texture yield five concordia ages, including 519.9 ± 4.6 Ma (MSWD = 0.57) for grains D49–50, 645 ± 5.3 Ma (MSWD = 4.2) for grains D52–53, 776.4 ± 4.4 Ma (MSWD = 1.9) for grains D55–58, 849 ± 5.5 Ma (MSWD = 6.6) for grains D59–60, 1203 ± 35 Ma (MSWD = 1.3) for grains D62–63, and 1489 ± 6.1 Ma (MSWD = 3.4) for grains D64–65 (Fig. 7e).

5.2.3. Shuangchagou mica gneiss and granite

Zircons from the mica gneiss SCG3 are classified into magmatic zircon and inherited zircon. The magmatic zircons are euhedral, transparent and colorless, have gray to dark gray color in the CL images, and are equant to short prismatic with lengths ranging from 60 to 120 μm and length/width ratios of 1:1 to 2.5:1 (Fig. 5e). The magmatic zircons have 258–3341 ppm U, 147–1152 ppm Th and 23–269 ppm Pb with Th/U ratios in the range of 0.186–0.904, $^{206}Pb/^{238}U$ ages ranging from 434.7 ± 6.3 Ma to 463.7 ± 6.9 Ma (Supplementary Table 3), $^{176}Hf/^{177}Hf$ values from 0.282213 to 0.282589, $\varepsilon_{Hf\ (t)}$ values from −10.4 to +3.2, and variable T_{DM1} (941–1469 Ma), T_{DMC} (1236–2084 Ma) and T_{DM2} (1232–2079 Ma) for 21 analyzed grains (Supplementary Table 4). Among these 21 analyzed magmatic grains, grains S1–8 are without zoning and have a concordia age of 436.8 ± 2.1 Ma (MSWD = 3.8), whereas grains S15–21 have clear oscillatory zoning and a concordia age of 458.6 ± 2.5 Ma (MSWD = 3.1) (Fig. 8a,b). The inherited zircons are euhedral to subhedral and could be divided into three populations: short prismatic with weak zoning and dark gray color in the CL images (population A), equant to prismatic with clear zoning and gray color in the CL images (population B) and equant and weak rounded with no internal zoning and slate gray color in the CL images (population C). The population A zircons (spots S22–29) have 364–2333 ppm U, 145–1267 ppm Th and 49–633 ppm Pb with Th/U ratios in the range of 0.258–0.714, $^{207}Pb/^{206}Pb$ ages ranging from 805.4 ± 25.4 Ma to 1465.1 ± 11.1 Ma that define a discordia line with an upper intercept age of 1472 ± 42 Ma (MSWD = 4.5; Supplementary Table 3, Fig. 8a), $^{176}Hf/^{177}Hf$ values from 0.282031 to 0.282463, $\varepsilon_{Hf\ (t)}$ values from +0.9 to +13.9, and variable T_{DM1} (1122–1714 Ma), T_{DMC} (1096–1893 Ma) and T_{DM2} (1098–1882 Ma) for 8 analyzed grains (Supplementary Table 4). The population B zircons (spots S30–32) have 357–794 ppm U, 56–478 ppm Th and 135–268 ppm Pb with Th/U ratios in the range of 0.122–0.603, $^{207}Pb/^{206}Pb$ ages ranging from 1724.7 ± 9.8 Ma to 1794.1 ± 10.9 Ma that define a discordia line with an imprecise upper intercept age of 1800 ± 160 Ma (MSWD = 13; Supplementary Table 3, Fig. 7a), $^{176}Hf/^{177}Hf$ values from 0.282591 to 0.282669, $\varepsilon_{Hf\ (t)}$ values from −0.9 to −4.4, and similar T_{DM1} (2215–2323 Ma), T_{DMC} (2534–2710 Ma) and T_{DM2} (2511–2682) for 3 analyzed grains. The population C zircons (spots S33–38) have 84–2710 ppm U, 110–600 ppm Th and 15–1131 ppm Pb with Th/U ratios in the range of 0.101–2.437, a $^{206}Pb/^{238}U$ age of 437.3 ± 6.4 Ma, $^{207}Pb/^{206}Pb$ ages ranging from 2115.8 ± 16 Ma to 2498.4 ± 4.5 Ma that define a discordia line with an upper intercept age of 2476 ± 47 (MSWD = 16), $^{176}Hf/^{177}Hf$ values from 0.281153 to 0.282924, $\varepsilon_{Hf\ (t)}$ values from −20.5 to −2.1, and variable T_{DM1} (1830–2930 Ma), T_{DMC} (2714–3232 Ma) and T_{DM2} (2714–3200 Ma) for 6 analyzed grains. All the three zircons populations have similar lower intercept ages to a metamorphic age of the mica gneiss, implying that these zircons suffered the same metamorphism.

Zircons from the granite SCG2 are divided into magmatic zircon and inherited zircon as well. The magmatic zircons are euhedral, transparent and colorless, have a gray color and clear oscillatory zoning in the CL images, and are short to long prismatic with lengths ranging from 80 to 200 μm and length/width ratios of 1.5:1 to 4.5:1 (Fig. 5f). The magmatic zircons have 71–3111 ppm U, 16–333 ppm Th and 3–152 ppm Pb with Th/U ratios in the range of 0.034–0.852, $^{206}Pb/^{238}U$ ages ranging from 268.4 ± 4.2 Ma to 287.0 ± 4.2 Ma with a concordia age of 276.1 ± 1.1 Ma (MSWD = 0.21; Fig. 8c,d), $^{176}Hf/^{177}Hf$ values from 0.282243 to 0.283017, $\varepsilon_{Hf\ (t)}$ values from −14.1 to +14.3, and variable T_{DM1} (347–1485 Ma), T_{DMC} (386–2195 Ma) and T_{DM2} (386–2197 Ma) for 15 analyzed grains (Supplementary Table 4). A distinctive population A of inherited zircons were identified, and they are euhedral, have dark gray color and blurred to no zoning in the CL images and are short prismatic with lengths ranging from 80 to 120 μm and length/width ratios of 1.5:1 to 3:1. Population A has 211–2990 ppm U, 142–933 ppm Th and 19–238 ppm Pb with Th/U ratios in the range of 0.256–0.272, $^{206}Pb/^{238}U$ ages ranging from 428.5 ± 6.3 Ma to 445.5 ± 6.4 Ma with a concordia age of 433.5 ± 1.9 Ma (MSWD = 0.39; Fig. 8e), $^{176}Hf/^{177}Hf$ values from 0.282069 to 0.282486, $\varepsilon_{Hf\ (t)}$ values from −15.8 to −1.0, and variable T_{DM1} (1086–1685 Ma), T_{DMC} (1485–2417 Ma) and T_{DM2} (1480–2485 Ma) for 11 analyzed grains (spot G16–26). The other analyzed inherited zircons are euhedral to subhedral, have a gray to dark gray color and clear or weak zoning in the CL images, and are equant to short prismatic with length ranging from 70 to 110 μm and length/width ratios of 1:1 to 2:1. These zircons have 144–3837 ppm U, 7–1536 ppm Th and 26–985 ppm Pb with Th/U ratios in the range of 0.010–1.742, $^{206}Pb/^{238}U$ ages ranging from 568.9 ± 8.2 Ma to 809 ± 11.9 Ma, $^{207}Pb/^{206}Pb$ ages ranging from 927.4 ± 6.8 Ma to 2607.5 ± 2.7 Ma, $^{176}Hf/^{177}Hf$ values from 0.281196 to 0.282392, $\varepsilon_{Hf\ (t)}$ values from −25.1 to +6.8, and variable T_{DM1} (1196–2937 Ma), T_{DMC} (1488–3290 Ma) and T_{DM2} (1479–3253 Ma) for 20 analyzed grains (spot G27–46). Among these 20 analyzed inherited grains, grains G31, G32 and G35 (population B) have a short prismatic morphology, weak zoning and gray color in the CL images that define a discordia line with an upper intercept age of 957 ± 47 Ma (MSWD = 0.00; Fig. 8c); grains G39–41 (population C) have a similar subhedral and equant to short prismatic morphology,

gray color in the CL images, and a concordia age of 1135 ± 23 Ma (MSWD = 0.20); and ten grains have concordia ages of 568.9 ± 8.2 Ma (spot G27), 589.9 ± 8.5 Ma (spot G28), 611.6 ± 8.8 Ma (spot G29), 681.6 ± 9.7 Ma (spot G30), 788.9 ± 11.1 Ma (spot G33), 809.0 ± 11.9 Ma (spot G34), 973.7 ± 13.6 Ma (spot G36), 1011.5 ± 14.2 Ma (spot G37), 1055.5 ± 14.6 Ma (spot G38) and 1636.9 ± 21.8 Ma (spot G43).

6. Discussion

6.1. Basement nature of the Junggar terrane

6.1.1. Crust basement in the Taheir area

The enclave gneisses are possibly metamorphosed from diorites on the basis of the following evidence: 1) most zircons from the gneiss enclave TH4-1 are euhedral to subhedral and some have a clear oscillatory zonation of magmatic zircons (Corfu et al., 2003); 2) the gneiss has a geochemical composition of diorite with SiO_2 at 53.37 wt.% and ($Na_2O + K_2O$) at 3.41 wt.% (Le Bas et al., 1986); and 3) the gneiss mainly consists of hornblendes and andesites, which are the primary minerals of diorites (Best and Christiansen, 2001). The age of approximately 2.52 Ga is combination of the concordia age of 2522.5 ± 16 Ma of the 3 euhedral zircons with a clear oscillatory zoning and the upper intercept age of 2517 ± 23 Ma of the discordia line defined by 11 euhedral zircons and may represent a formation age of the protolithic diorite, whereas the age of approximately 1.88 Ga is a combination of the concordia age of 1877.2 ± 10 Ma of 9 zircons and the upper intercept age of 1891 ± 36 Ma of the discordia line defined by 11 zircons and shows a metamorphic age of the dioritic gneiss. Therefore, the 1.88 Ga gneisses were formed by metamorphism of 2.52 Ga diorites. Evidence that the magmatic zircons have variable $\varepsilon_{Hf\,(t)}$ and T_{DM} ranging from a ~2.52 Ga mantle-derived melt to a ~3.1 Ga crust indicates that the 2.52 Ga diorites were likely produced by a mixing of the 2.52 Ga mantle-derived melts and 3.1 Ga crust (Fig. 9a), which suggests existence of a ~3.1 Ga crust in the Taheir area.

There is evidence that the zircons from the magnetite quartzite interlayered with the hornblende–plagioclase gneiss layers (enclave TH4-2) have consistent ages that plot on a discordia line with an upper intercept age of 1929 ± 14 Ma or on the crust evolution line with the concordia age of 1916.9 ± 4.8 Ma (Fig. 6b). In addition, and most zircons have similar subhedral to anhedral morphology with blurred or weak zoning, which indicates that these zircons are magmatic and possibly separated from the interlayers of hornblende–plagioclase gneisses because the magnetite quartzite, which is a chemical sedimentary rock, generally contains rare detrital zircons with various ages (James, 1954), whereas the hornblende–plagioclase gneiss that is interlayered with a composition of hornblende, andesine, quartz and magnetite was possibly metamorphosed from intermediate tuff (Winter, 2001). Based on the assumption that the age of the zircons from the tuff interlayers of magnetite quartzite may represent a formation age of the magnetite quartzite (Pickard, 2002, 2003), it is suggested that the magnetite quartzite with interlayers of hornblende–plagioclase gneisses was formed at approximately 1.92 Ga, which is a combination by the concordia age of 1916.9 ± 4.8 Ma of 7 zircon grains and the upper intercept age of 1929 ± 14 Ma of the discordia line defined by 22 zircons. A relatively concentrated $\varepsilon_{Hf\,(t)}$ and T_{DM} with T_{DMC} of 2817–

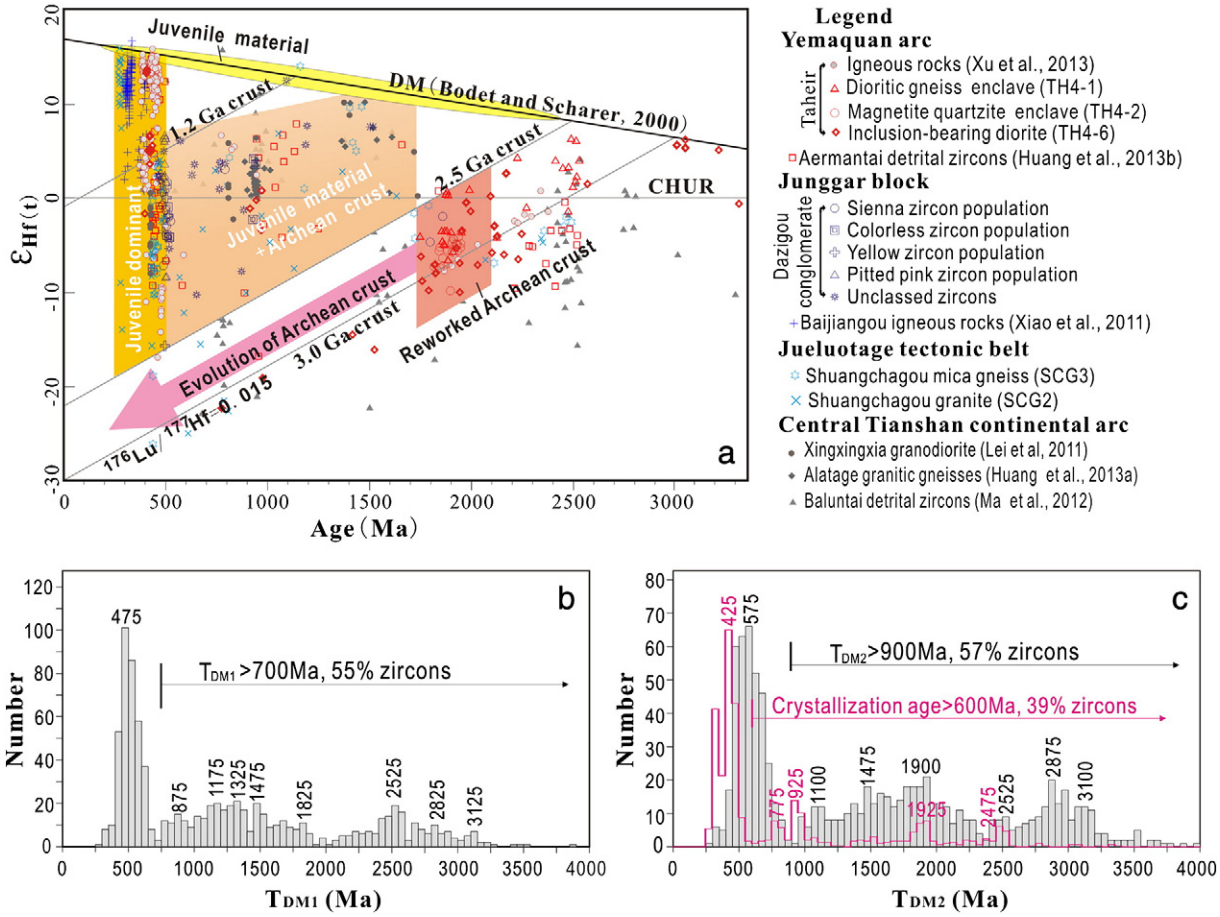

Fig. 9. Diagram of the $\varepsilon_{Hf\,(t)}$ versus U–Pb age (a) and histograms of the Hf depleted mantle model ages of T_{DM1} (c) and T_{DM2} (d) for the zircons from the Junggar terrane. The corresponding relative U–Pb age probability for these zircons is shown by the red histogram in panel d. The data for panel b are from this study, and the data for panels c and d are mentioned in the legend of panel a. The depleted mantle (DM) growth curve from Bodet and Scharer (2000). CHUR, chondritic uniform reservoir.

3128 Ma and T_{DM2} of 2788–3144 Ma indicates that these zircons and their 1.92 Ga host tuff interlayers were dominantly formed by the melting of a ~3.1 Ga crust with a minor input of mantle-derived melts. This also shows the existence of a ~3.1 Ga crust in the Taheir area. There is evidence that the concordia age (419.0 ± 5.5 Ma) of the diorite TH4-6 is consistent with the lower intercept ages of both the dioritic gneiss TH4-1 and magnetite quartzite TH4-2, indicating that an alteration of the U–Pb–Th isotopes of some zircons that form these two enclaves was possibly induced by the 419 Ma diorite.

There is evidence that most of the inherited zircons from the diorite TH4-6 are euhedral to subhedral with clear or weak zoning and without pits at the grain surfaces (Fig. 5c), which indicates that these inherited zircons are mostly magmatic or metamorphosed magmatic (Corfu et al., 2003). The inherited zircons were possibly derived from the wall rocks that the diorite passed through, or they were possibly gravels or detrital zircons from a neighboring provenance because the long distance transport of zircons from provenances by a river will cause these zircons to be rounded and pitted (Gärtner et al., 2013). This suggests that these euhedral to subhedral inherited zircons were possibly from the wall or adjacent magmatic or metamorphosed magmatic rocks. The occurrence of zircon couples and populations with similar morphology and internal texture greatly enhances the existence of rocks with an age yielded by the zircons. Based on this assumption, the Taheir basement that is indicated by the inherited zircons from the diorite TH4-6 contains magmatic rocks with ages of approximately 3.06 Ga, 2.13 Ga, 2.02 Ga, 1.98 Ga, 1.69 Ga, and 0.98 Ga and metamorphic rocks with an age of approximately 1.89 Ga. The upper intercept age of 1.89 Ga defined by the metamorphosed zircon population A (Grain R17, R22 and R26–28) is consistent with the metamorphic age of approximately 1.88 Ga of the dioritic gneiss TH4-1. The occurrence of zircon grain 49 with a $^{207}Pb/^{206}Pb$ age of approximately 3.32 Ga indicates that the Taheir basement contains 3.32 Ga materials.

The Hf isotope evidence of the Taheir zircons from this study and the reference of Xu et al. (2013) shows the following facts (Fig. 9a): 1) there is an Archean basement with 3.22–3.06 Ga mantle-derived magmatic rocks in the Taheir area, and the Taheir crust was possibly formed at 3.22–3.06 Ga; 2) the 2.52 Ga diorite possibly originated from a mixture of a juvenile and 3.22–3.06 Ga crust, whereas the 2.5–1.7 Ga zircons, their host rocks and 1.92 Ga magnetite quartzite interlayered with the hornblende–plagioclase gneiss layers originated from a reworking of the Archean crust; and 3) the Taheir Archean crust underwent three distinctive evolution stages and processes, which included a 2.1–1.7 Ga reworking of the Archean crust, Mesoproterozoic–Neoproterozoic weaker magmatism with a mixture between a juvenile and the Archean crust, and Paleozoic continental arc-type juvenile dominant mixture with the Archean crust between 480 and 390 Ma (Fig. 9a).

The above zircon U–Pb–Hf isotopes indicate that the Taheir basement has an Archean crust consisting of a 3.22–3.06 Ga juvenile crust with 2.52 Ga intrusive bodies. The Archean crust was reworked to form the 2.13 Ga, 1.98 Ga, 1.77 Ga and 1.69 Ga igneous rocks and 1.92 Ga magnetite quartzite with tuff interlayers. The Archean basement provided materials for the Mesoproterozoic to Paleozoic igneous rocks in the Taheir area. The Taheir basement experienced a series of Precambrian magmatic evens with ages of approximately 2.52Ga, 2.13 Ga, 1.98 Ga, 1.89 Ga, 1.77 Ga, 1.65Ga, 1.55Ga, 0.98Ga and 0.78Ga, and suffered metamorphism at approximately 1.88 Ga when the 2.52 Ga diorites were metamorphosed to form the enclave gneisses.

6.1.2. Crust basement in the Dazigou area

Although it is difficult to relate the sienna, colorless, yellow and pink zircon populations separated from the conglomerate DZG1 to the four certain pebbles, the morphology and internal textures of these zircons could reveal their origins. The sienna, colorless and yellow populations with euhedral to subhedral morphology and clear to weak zonation were most likely separated from three different magmatic or metamorphosed magmatic rock pebbles from the Dazigou area, whereas the pink zircon population with pitted surfaces that has a subhedral to subrounded morphology and clear oscillatory zoning was possibly a type of detrital zircon that separated from a magmatic rock and was possibly transported by a river for a long distance. Therefore, the zircon U–Pb–Hf isotope evidence of the sienna, colorless and yellow populations could add to the understanding of the nature of the crust basement of the Dazigou area.

There is evidence that the sienna euhedral zircon (grain D1) with weak zonation, 562 ppm U, 395 ppm Th, Th/U ratio of 0.702 and $^{176}Hf/^{177}Hf$ ratio of 0.281581 plots along the crust evolution line with a $^{206}Pb/^{238}U$ age of 1855 ± 24.2 Ma, and there is also evidence that some of the sienna resorbed zircons (grains D5–13) with elevated U contents ranging from 1413 to 4573 ppm, Th contents up to 1354 ppm and $^{176}Hf/^{177}Hf$ ratios ranging from 0.282278 to 0.282646, and lowered Th/U ratios between 0.44 and 0.038 have a lower concordia age of 503.9 ± 6.7 Ma, indicating that these resorbed zircons underwent fluid-involving metamorphic recrystallization (Hoskin and Black, 2000; Chen et al., 2010). Therefore, these sienna euhedral to subhedral zircons were most likely separated from a metamorphosed magmatic rock with a crystallization age of approximately 1.86 Ga and metamorphic recrystallization age of approximately 504 Ma. This result is consistent with the sienna zircon grain D2 having a similar $^{176}Hf/^{177}Hf$ ratio of 0.281525, elevated U content of 1433 ppm, Th content of 629 ppm, and lower Th/U ratio of 0.44 and U–Pb ages to the grain D1 and has a plot on a discordia line defined by the euhedral zircon grain D1 and resorbed zircon grains D5–13 with an upper intercept age of 1843 ± 22 Ma and lower intercept age of 505 ± 17 Ma (Fig. 7a). The occurrence of sienna zircon grains D3–4 with medium U and Th content, lowered Th/U ratio and U–Pb ages, and elevated $^{176}Hf/^{177}Hf$ ratios indicates that the magmatic rock containing the sienna zircon population suffered another metamorphic event with an age of approximately 0.74 Ga. There is evidence that the zircon grains D1 and D2 that plot along or close to the crust evolution line have a T_{DMC} of 2817–3128 Ma and T_{DM2} of 2788–3144 Ma, which indicates that the 1.86 Ga magmatic rocks are produced by a mixing of juvenile and ~3.1 Ga crust (Fig. 9a) and also confirms the ~3.1 Ga crust in the Dazigou area. Similarly, the colorless zircon population that has an euhedral and short to long prismatic morphology and weak zonation were possibly separated from a metamorphosed magmatic rock with a crystallization age of approximately 0.94 Ga and metamorphic recrystallization age of approximately 514 Ma. These interpretations and conclusions for the sienna and colorless zircon populations are consistent with the occurrences of gneiss and granitic mylonite pebbles in the conglomerates in the Dazigou area.

The yellow zircon population with a subhedral to anhedral morphology and weak zonation may represent a magmatic rock with an age of approximately 496 Ma, whereas the pink zircon population with euhedral to subhedral morphology, and clear or weak zonation records a magmatic event with an age of approximately 498 Ma. The unclassified euhedral to subhedral inherited zircons from the conglomerate DZG1 show that there is possibly a series of magmatic rocks with ages of approximately 1.80 Ga, 1.49 Ga, 1.20 Ga, 1.1 Ga, 0.85 Ga, 0.78 Ma, 0.65 Ga, 0.64 Ga, 0.63 Ga, 0.57 Ga, 520 Ma, 492 Ma, 478 Ma and 464 Ma in or adjacent to the Dazigou area. This suggestion is supported by the occurrence of a large number of tuff, porphyry and granite pebbles in the conglomerates in the Dazigou area. More recently, Long et al. (2012) showed that three graywackes of the Ordovician Huangcaopo group from three locations adjacent to the Dazigou area contain detrital magmatic zircons with peak ages of approximately 0.91 Ga, 0.93 Ga and 0.94 Ga.

The above zircon U–Pb–Hf isotopes indicate that the Dazigou crust possibly has an Archean basement with a ~3.1 Ga crust, and contains magmatic rocks with ages of 1.86 Ga, 1.80 Ga, 1.49 Ga, 1.20 Ga, 1.1 Ga, 0.94–0.91 Ga, 0.85 Ga, 0.78 Ma, 0.65–0.63 Ga, 0.57 Ga, 520 Ma, 498–492 Ma, 478 Ma and 464 Ma, and suffered metamorphism at 0.74 Ga, 514 Ma and 504 Ma. The 514 Ma and 504 Ma metamorphic events

and subsequent 492–498 Ma magmatism are possible records of an orogenic event in the Dazigou area.

6.1.3. Crust basement in the Shuangchagou area

There is evidence that the mica gneisses that have intrusive contacts with their ambient gneisses have the geochemical composition of a granodiorite with SiO_2 at 64.2 wt.% and ($Na_2O + K_2O$) at 6.18 wt. % (Le Bas et al., 1986) and contain magmatic zircons with euhedral morphology, indicating that these mica gneisses were possibly metamorphosed from granodiorite. A high content of mica is possibly related to the participation of fluids during metamorphism and deformation. The magmatic zircon grains S15–21 with clear oscillatory zoning from the mica gneiss SCG3 should record the crystallization age of their protolithic granodiorite, whereas the magmatic zircon S1–8 without zoning may present the metamorphic and recrystallization age of the gneiss. This would indicate that the mica gneisses were formed by the metamorphism of 459 Ma granodiorites at approximately 437 Ma. A variety of T_{DMC} from 1236 Ma to 2084 Ma and T_{DM2} from 1232 Ma to 2079 Ma for these magmatic zircons indicates that the Shuangchagou basement should be older than 1.2 Ga and possibly up to 2.08 Ga. The three inherited magmatic zircon populations show three magmatic events and rocks with ages of approximately 2.48 Ga, 1.80 Ga and 1.47 Ga.

The magmatic zircons with euhedral morphology and clear oscillatory zoning from the granite SCG2 reveal that the syn-tectonic granite pluton in the Shuangchagou area was emplaced at approximately 276 Ma. The evidence that these magmatic zircons have T_{DMC} and T_{DM2} up to 2.2 Ga also suggests that the Shuangchagou basement contains Precambrian crust. The evidence that the inherited zircon population A, which has a euhedral morphology and blurred to no zonation, similar to recrystallized magmatic zircons, has a similar concordia age of approximately 434 Ma and Hf isotope composition with the metamorphosed magmatic zircons from the mica gneiss SCG3 indicates that the zircon population A is possibly from another mica gneiss that was assimilated by the granite. The other inherited zircons with euhedral to subhedral morphology and clear or weak zoning are magmatic and possibly from the wall and source rocks of the granite (Corfu et al., 2003; Gärtner et al., 2013). These inherited zircons reveal the existence of Precambrian magmatic events and rocks with ages of approximately 1.64 Ga, 1.14 Ga, 1.06 Ga, 1.01 Ga, 0.97–96 Ga, 0.81–0.79 Ga, 0.68 Ga, 0.61 Ga, 0.59 Ga and 0.57 Ga in the Shuangchagou area.

The Hf isotope evidence of the Shuangchagou zircons shows the following facts (Fig. 9): 1) the Shuangchagou crust has a Paleoproterozoic basement with 2.48 Ga and 1.80 Ga magmatic rocks; 2) 2.48 Ga and 1.80 Ga magmatic zircons and their host rocks possibly originated from a reworking of Archean materials; and 3) Shuangchagou crust went through three distinctive evolution stages and processes, such as the formation of a Paleoproterozoic basement between 2.48 Ga and 1.80 Ga, magmatism with a mixture of juvenile and Archean materials between 1.70 Ga and 459 Ma, and a Paleozoic continental arc-type juvenile dominant mixture with Archean materials at 276 Ma in the Shuangchagou area (Fig. 9).

These zircon U–Pb–Hf isotopes indicate that the Shuangchagou crust has a Paleoproterozoic basement containing magmatic rocks with ages of approximately 2.48 Ga, 1.80 Ga, 1.64 Ga, 1.47 Ga, 1.14 Ga, 1.06 Ga, 1.01 Ga, 0.97–96 Ga, 0.79–0.81 Ga, 0.68 Ga, 0.61 Ga, 0.59 Ga, 0.57 Ga, 459 Ma and 276 Ma and suffered metamorphism at approximately 437–434 Ma.

6.1.4. Crust basement in the Kalamaili area

Li et al. (2007) reported that the Devonian sandstones in the Kalamaili area in the northeastern Junggar block contain Precambrian detrital zircons with SHRIMP U–Pb ages ranging from 550 Ma to 3073 Ma. After reexamining the data reported by Li et al. (2007), we found some new evidence: 1) the zircon grains 9.1, 70.1 and 71.1 are a population of metamorphic zircons with rounded morphology and Th/U ratios ranging from 0.12 to 0.27, and they have a concordia age of 953 ± 9.1 Ma (MSWD = 4.3); 2) zircon grains 3.1, 77.1 and 85.1 are magmatic zircons that have a subhedral morphology, clear zonation, Th/U ratios ranging from 0.26 to 0.48 and plots that define a discordia line with an upper intercept age of 2473 ± 23 Ma (MSWD = 0.83); and 3) zircon grain 12.1 has a similar elliptic morphology, weak zoning and gray color in the CL image, and $^{207}Pb/^{206}Pb$ age of 3073 ± 10 Ma to the inherited zircon population C that from the diorite TH4-4 from the Taheir area. This finding indicates that the Kalamaili crust possibly has an Archean basement with 3.07 Ga rocks and contains 2.47 Ga magmatic rocks and 0.95 Ga metamorphic rocks.

6.1.5. Basement nature beneath the Junggar basin

Recently, many studies (e.g., Zheng et al., 2007; Xiao et al., 2011; Su et al., 2012; Yang et al., 2012a, 2012b; D.F. He et al., 2013; and Li et al., 2014) reported the geochronology, geochemistry, multichannel seismic reflection data and tectonostratigraphy of Carboniferous rocks beneath and adjacent to the Junggar basin. The tectonic setting of these rocks is related to either the oceanic crust (Zheng et al., 2007), volcanic arc (Yang et al., 2012b), oceanic island arc (Xiao et al., 2011; Su et al., 2012; D.F. He et al., 2013), or continental arc (Yang et al., 2012a). After carefully reexamining this published data, we found that certain interpretations were incorrect.

Zheng et al. (2007) suggested that the Carboniferous volcanic rocks beneath the Junggar basin is derived from an oceanic crust based on the conclusions of Condie (1999), who stated that the oceanic crust (MORB + OIB) could be distinguished from arc volcanic rocks by a low La/Nb ratio (<1.4). However, a ratio of La/Nb < 1.4 is not exclusive to the oceanic crust (MORB + OIB); arc volcanic rocks can have a low La/Nb ratio (<1.4) (Fig. 4 of Rudnick, 1995; Fig. 2 of Condie, 1999; Fig. 5 of Condie, 2000) and some MORBs may have intermediate La/Nb ratios (>1.4) up to 2.5 (Fig. 2 of Le Roux, 1986; Fig. 5 of Jahn et al., 1999). Therefore, Condie (1999, 2000) combined a La/Nb ratio (<1.4) and Ni concentration (>30 ppm at an Mg number of 40) to distinguish the MORBs from the arc volcanic rocks (Fig. 1 of Condie, 1999; Fig. 7 of Condie, 2000). Indeed, data published by Zheng et al. (2007) shows that some basalts (samples k178, k204 and k211) have La/Nb ratios equal to or greater than 1.4 (Fig. 6 of Zheng et al., 2007), and most basalts have very low Ni_{40} (<22 ppm) (Table 2 and Fig. 9 of Zheng et al., 2007), which indicates that this data does not support the interpretations of Zheng et al. (2007). Moreover, almost all of the published geochemical data for the Carboniferous igneous rocks beneath and adjacent to the Junggar basin shows that they are most likely related to arc setting rather than oceanic crust. For example, they have an arc-type enrichment in Pb, depletion in Nb and element spider patterns (Fig. 7 of Zheng et al., 2007; Fig. 8 of Xiao et al., 2011; Fig. 8 of Su et al., 2012; Fig. 11 of Yang et al., 2012a; Fig. 8 of Yang et al., 2012b; Fig. 7 of D.F. He et al., 2013; Hofmann, 1988; Rudnick, 1995; Winter, 2001; Albarède, 2003). They also have a lower Ce/Pb ratio (<20) that plots in the continental crust (arc) field in the Ce/Pb versus Pb diagram (Fig. 10a; Hofmann, 1988), high Ba/Nb (>20) and La/Nb ratios (>1) that plots in or near the continental crust (arc) field in the Ba/Nb versus La/Nb diagram (Fig. 10b; Jahn et al., 1999; Fig. 9 of Zheng et al., 2007), lower Rb, Y and Nb content that plots in the volcanic arc granite (VRG) and within-plate granite (WPG) fields in the Rb versus Y + Nb diagram (Fig. 10c; Fig. 10 of Zheng et al., 2007; Fig. 9 of Xiao et al., 2011; Pearce et al., 1984; Fig. 13 of Yang et al.;, 2012b). All of the Late Paleozoic volcanic rocks plot in the field close to the lower crust and away from MORB and OIB in the $(^{206}Pb/^{204}Pb)_{initial}$ versus $(^{207}Pb/^{204}Pb)_{initial}$ and $(^{208}Pb/^{204}Pb)_{initial}$ diagram (Figs. 8c,d of Zheng et al., 2007). There are no or few plots in the MORB or OIB field in the Ce/Pb versus Pb, Ba/Nb versus La/Nb, Rb versus Y + Nb, and Th/Yb versus Ta/Yb diagrams (Fig. 10).

Additionally, the intermediate-felsic igneous rocks beneath and adjacent to the Junggar basin are enriched in U, Th, K, Zr and Pb, depleted in Nb, P and Ti (Fig. 8 of Xiao et al., 2011; Fig. 8 of Su et al., 2012), have

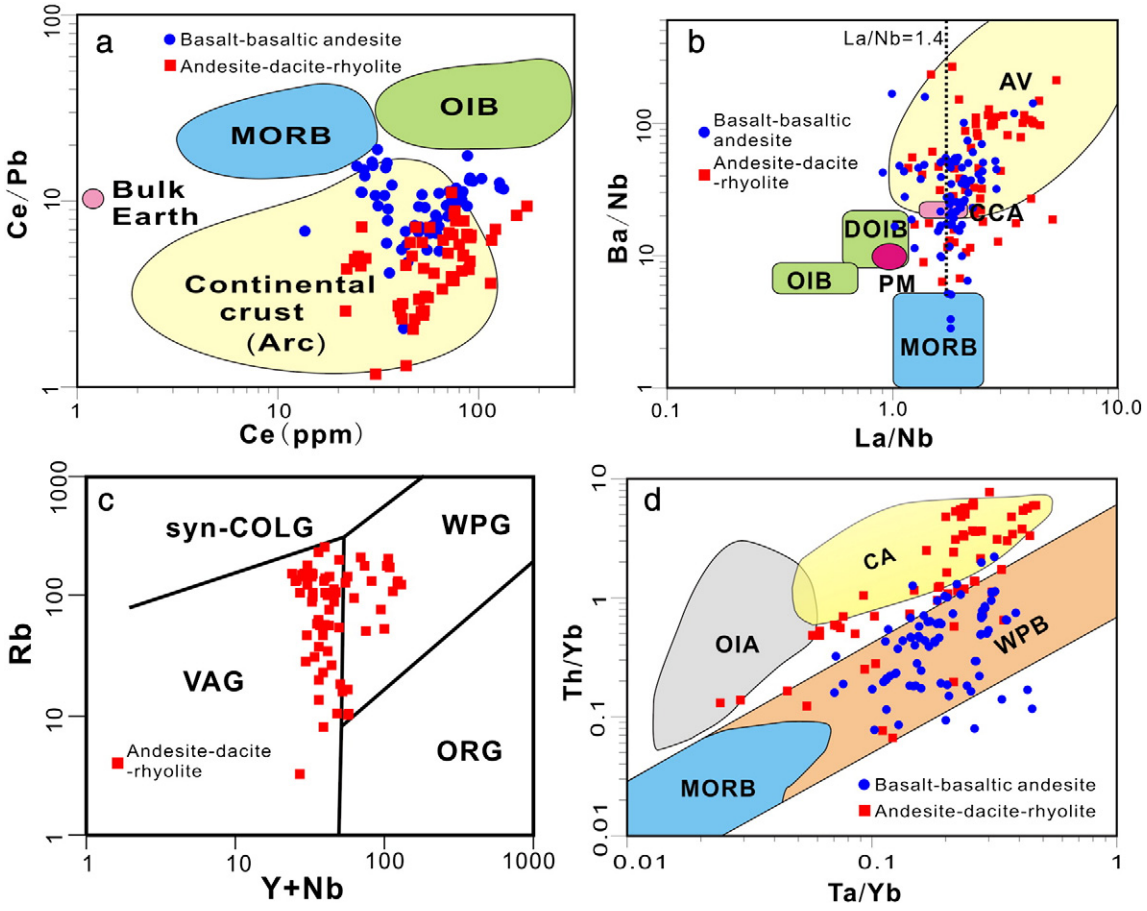

Fig. 10. (a) Ce/Pb versus Ce diagram (after Hofmann, 1988), (b) Ba/Nb versus La/Nb diagram (after Jahn et al., 1999), (c) Rb versus Y + Nb diagram (after Pearce et al., 1984) and Th/Yb versus Ta/Yb diagram (after Pearce and Norry, 1979) for the Carboniferous igneous rocks beneath and adjacent to the Junggar basin. Data source for the Carboniferous volcanic rocks beneath and adjacent to the Junggar basin is after Zheng et al.(2007), Xiao et al. (2011), Su et al. (2012), Yang et al. (2012a, 2012b), D.F. He et al. (2013) and Li et al. (2014). AV: arc volcanic rocks; CA: continental arc; CCA: continental crust average; DOIB: Dupal oceanic island basalt; OIA: oceanic island arc; MORB: midocean ridge basalts; OIB: oceanic island basalt; ORG: ocean ridge granites; PM: primitive mantle; syn-COLG: syn-collision granites; VAG: volcanic arc granites; WPB: within plate basalts; WPG: within plate granites.

high ratios of Th/Yb and Ta/Yb (Fig. 10d; Fig. 12 of Su et al., 2012) and negative Eu anomalies. This geochemical signature indicates that they are possibly related to the continental arc rather than the oceanic island arc because igneous rocks formed at oceanic island arcs are usually enriched in Sr, Th and P, and depleted in Zr (Bailey, 1981; Ellam and Hawkesworth, 1988; Pearce and Norry, 1979; Winter, 2001). This conclusion is supported by the following evidence: 1) there are abundant Precambrian inherited zircons in tuff (sample LD1) in the Luliang area, and six grains (grain 6, 8, 9, 10, 13 and 14) of these zircon grains yield a discordia line with an imprecise upper intercept age of 1825 ± 170 Ma (MSWD = 47) (Table 1 of Yang et al., 2012a); 2) some zircons from magmatic rocks in the Baijiangou and Zhangpenggou areas have $\varepsilon_{Hf\ (t)}$ values close to zero and $T_{DM(Hf)}$ ages up to 1.3 Ga (Table 1 and Fig. 7 of Xiao et al., 2011); and 3) the Carboniferous sedimentary rocks in the Luliang area suggest a continental island arc to active continental margin setting (Fig. 12 of Yang et al., 2012b). Therefore, it could be concluded that there is possibly a Precambrian basement with a 1.83 Ga crust beneath the Junggar basin; however, the detailed basement nature (i.e., age and context) beneath the Junggar basin must be made clear in the future.

Furthermore, new statistical results in published geochemical data shows that these Carboniferous volcanic rocks are bimodal (Fig. 11a) and have plots that are in a broad area in or close to the continental arc and back-arc basin field in a newly created La × Th versus Nb/Th diagram (Fig. 11b), in which volcanic rocks from the MORB, OIB, continental arc, oceanic island arc and back-arc basin could be discriminated. These signatures are similar to those of volcanic rocks formed in the Mississippian continental intra-arc rift setting (Fig. 11; Simard et al., 2007), implying that the Carboniferous volcanic rocks beneath and adjacent to the Junggar basin were possibly formed in a continental intra-arc rift to back-arc basin setting as well. This conclusion is supported by existence of the EW-trending Carboniferous Luliang volcanic basin that is revealed by the multichannel seismic reflection profiles reported by Yang et al. (2012b) (Fig. 12). The occurrence of the EW-trending Carboniferous Luliang volcanic basin at a westward extension of the Kelameili ophiolite zone indicates that the Kelameili ophiolite zone possibly represents relicts of the Junggar arc-back ocean (Dong et al., 2009).

6.1.6. Crust basement of the Central Tianshan crust

The published U–Pb–Hf isotopes of magmatic zircons and Sm–Nd isotopes of gneisses from the Central Tianshan mountain indicate that the Central Tianshan crust has a 1.7–1.85 Ga basement that contains Precambrian intrusives with ages of approximately 1.54 Ga, 1.40–1.41 Ga, 0.95 Ga, 0.94 Ga, 0.93 Ga, 0.92 Ga and 0.81 Ga and suffered metamorphism at approximately 1.1–0.9 Ga (e.g., Hu et al., 2000, 2006; Li et al., 2007; Su et al., 2008; Chen et al., 2009; Q.G. Li et al., 2009; Hu et al., 2010; Lei et al., 2011; Z.Y. He et al., 2013). Recently, Ma et al. (2012) reported that the Precambrian detrital zircons from the Ordovician metasedimentary rocks in the Baluntai area have peak ages of approximately 2.46 Ga, 1.86 Ga, 1.57 Ga, 0.96 Ga, 0.81 Ga, 0.75 Ga and 0.56 Ga. The 2.46 Ga detrital zircons are suggested as originating from far places near to the Shuangchagou area or the Kalamaili area based on the following evidence: 1) the South Tianshan ocean

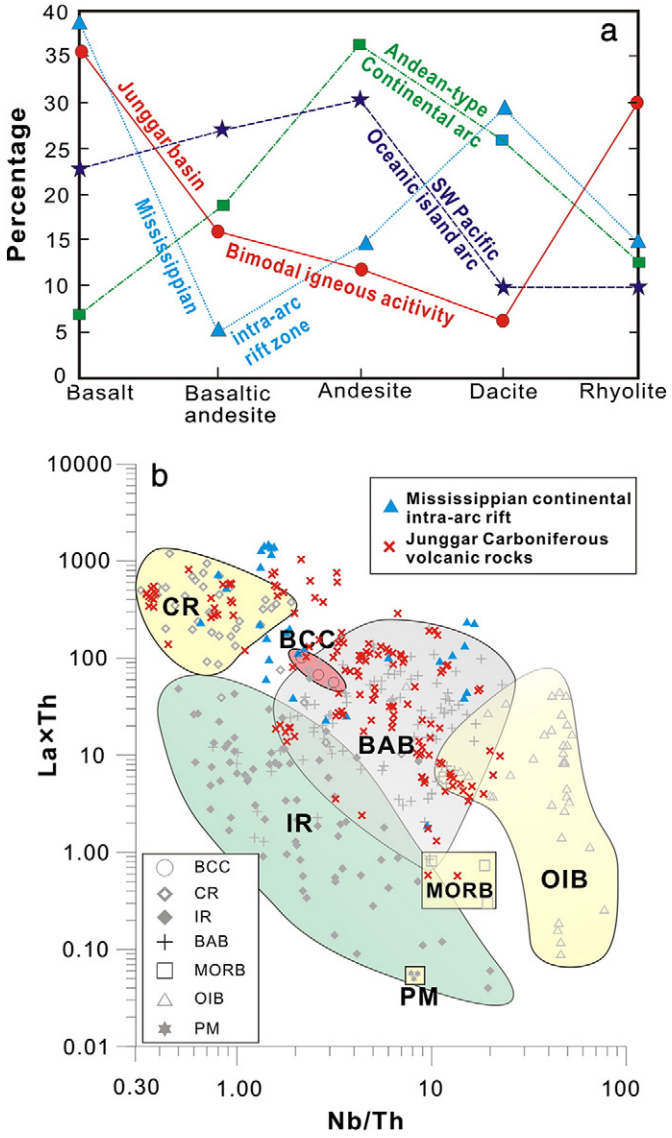

Fig. 11. Relative frequency of rock types (a) and the La × Th versus Nb/Th diagram (b) for the Carboniferous volcanic rocks beneath and adjacent the Junggar basin. The Andes continental arc, SW Pacific island arcs and Mississippian intra-arc rift volcanic rocks (Winter, 2001; Simard et al., 2007) are present in panel a for comparison, whereas Mississippian intra-arc rift volcanic rocks (Simard et al., 2007) are present in panel b for comparison. The data source for the Carboniferous volcanic rocks beneath and adjacent the Junggar basin is the same as that of Fig. 10. Data source for fields in panel b: BCC (Bulk continental crust), PM (primitive mantle) and MORB average (Weaver and Tarney, 1984; Taylor and McLennan, 1985; Hofmann, 1988; McDonough and Sun, 1995; Rudnick and Fountain, 1995), BAB (back-arc basin; Price et al., 1990; Stern et al., 1996; Keller et al., 2002; Koloskov et al., 2011), CR (continental arc; Chiaradia et al., 2004; Goss et al., 2011), IR (oceanic island arc; Bailey et al., 1989; Greene et al., 2006; Martynov et al., 2010), OIB (Regelous et al., 2003).

presented by the South Central Tianshan ophiolite belt south to the Baluntai area was possibly opened before the Ordovician and closed during the Carboniferous–early Permian (e.g. Gao et al., 2009, 2011; Biske and Seltmann, 2010; Glorie et al., 2011), and the detrital zircons from the Ordovician–Carboniferous sedimentary rocks possibly did not originate from the Tarim craton south of the South Tianshan Ocean; 2) the rounded morphology of the 2.46 Ga detrital zircons requires a long distance transport; 3) there are 2.48 Ga magmatic rocks in the Shuangchagou area and 2.47 Ga magmatic rocks in the Kalamaili area. Therefore, the Central Tianshan crust possibly has a 1.86–1.7 Ga basement and is characterized by extensive magmatic activities at approximately 1.57–1.54 Ga, 1.41–1.40 Ga, 0.97–0.92 Ga and 0.81–0.75 Ga.

6.1.7. Significance of Precambrian zircons from the Aermantai ophiolitic mélange

Most recently, Huang et al. (2013) reported on the LA-ICP-MS ages of detrital zircons from the Late Silurian sedimentary sequences in the Aermantai ophiolitic mélange; they found that more than half of the detrital zircons (79 grains of 142 analyzed zircons) were Precambrian with $^{207}Pb/^{206}Pb$ ages ranging from 582 Ma to 4.0 Ga. These detrital zircons were interpreted as being derived from the Altai orogen in the north by Huang et al. (2013). However, the Silurian–Carboniferous Erqis ophiolitic zone and Devonian–Carboniferous Sawuer oceanic island arc are between the Altai orogen and Aermantai ophiolitic mélange (Dong et al., 2009; Wong et al., 2010), which implies that there is a huge Paleo-Asian ocean between the Altai orogen and Aermantai ophiolitic mélange from the Silurian to Carboniferous. This indicates that these Precambrian detrital zircons in the Late Silurian sedimentary sequences in the Aermantai ophiolitic mélange could not have been transported from the Altai orogen. This conclusion is supported by the age spectra of the Precambrian zircons in the Aermantai ophiolitic mélange, which have more similar peak ages with those of the Junggar terrane between the Aermantai ophiolite zone and south Tianshan suture than the Altai orogen (Fig. 13). Alternatively, the Aermantai Precambrian detrital zircons could have been derived from the Junggar terrane south of the Aermantai ophiolitic mélange; this suggestion is consistent with the evidence that some detrital zircons in the Baluntai area have $T_{DM(Hf)}$ ages close to 4.0 Ga (Ma et al., 2012). The occurrence of 4.0 Ga zircons in the Late Silurian sedimentary sequences in the Aermantai ophiolitic mélange suggests that the Junggar terrane with 4.0 Ga crust materials could have been a part of an ancient continent containing a 4.0 Ga crust.

6.1.8. Crust basement of the Sawuer arc

As mentioned above, the Sawuer oceanic island arc to the south of the Erqis suture is characterized by the occurrence of Devonian adakites, porphyry Cu–Au deposits and Nb-enriched basalts, and developed on an Ordovician–Devonian juvenile crust (Zhang et al., 2004, 2006; Dong et al., 2009; Z.C. Zhang et al., 2009). The formation of the Sawuer oceanic island arc is related to intra-oceanic southward subduction of the Paleo-Asian oceanic plate (Xu et al., 2013). Thus, the Sawuer arc has a basement of Ordovician–Devonian juvenile crust.

6.1.9. Precambrian basement and tectonic belts of the Junggar terrane

Statistical results of the analyzed zircons that are broadly from the Junggar terrane from the Aermantai ophiolite mélange to Central Tianshan range show that 39% of the zircons have a crystallization age of more than 600 Ma, and 57% of the zircons have a T_{DM2} age greater than 900 Ma, and 55% of the zircons have a T_{DM1} age greater than 700 Ma (Fig. 9b,c); this evidence implies that more than half of the materials for the crust of the Junggar terrane between the Aermantai subduction zone and south Tianshan suture are Precambrian and the Junggar terrane could have an essentially Precambrian basement. Histograms of the T_{DM1} and T_{DM2} for these zircons have similar peak ages, respectively, of 3125 or 3100 Ma, 2875 or 2825 Ma, 2525 Ma, 1900 or 1825 Ma, 1475 Ma, 1325 Ma, 1175 Ma, 1100 Ma, and 575 or 475 Ma for the potential crust growth and magmatic and metamorphic events. The above features of the Precambrian basement, magmatism and metamorphism in the Taheir, Dazigou, Shuangchagou, Kalamaili, Aermantai and Central Tianshan area indicate that the Junggar terrane has three Precambrian basement units and diversiform magmatic and metamorphic belts that are regularly presented between the Hongguleleng–Aermantai subduction zone and south Tianshan suture (Fig. 14). There is a 2.1–1.7 Ga reworked Archean crust consisting of 3.22–3.06 Ga juvenile crust with 2.52 Ga diorite and ~4.0 Ga materials in the Taheir–Kalamaili–Dazigou area, 2.5–1.8 Ga crust in the Shuangchagou–Luliang area, and 1.86–1.7 Ga crust in the Tianshan area from north to south. There is possibly a 1.9–1.8 Ga orogen that is

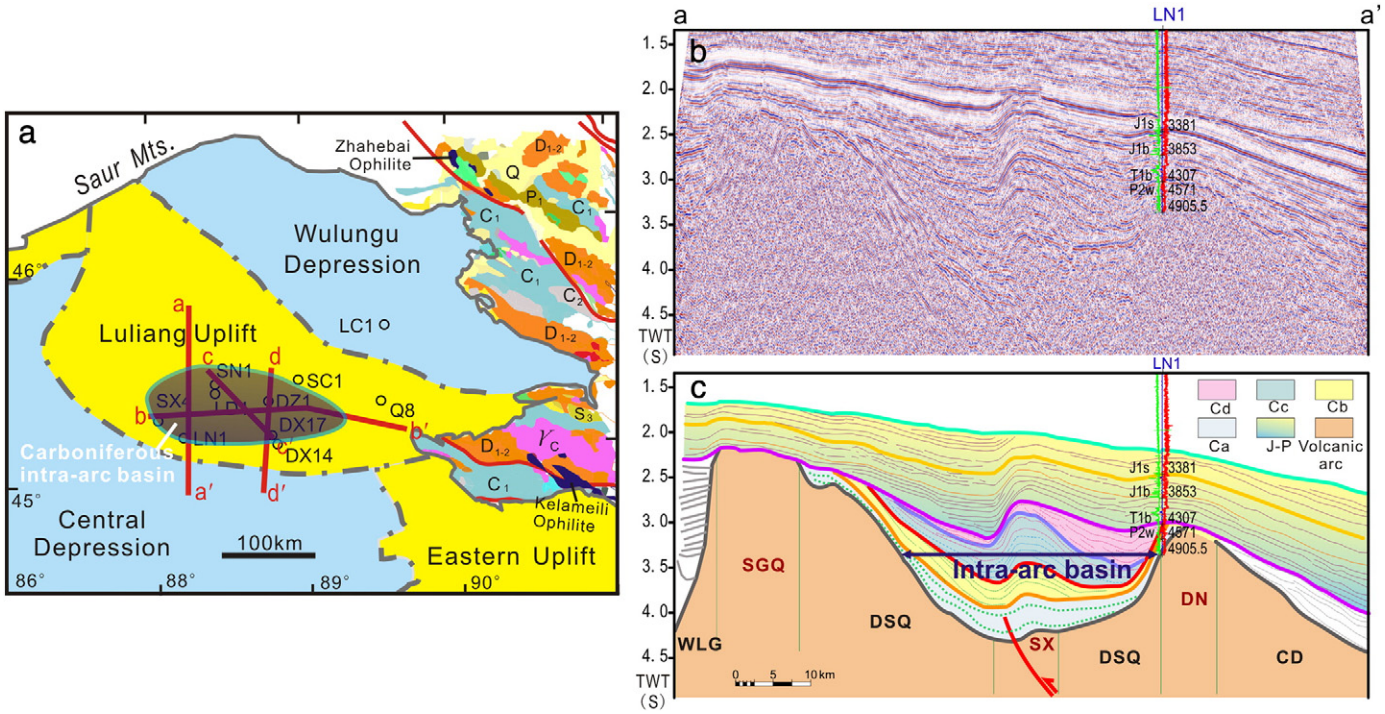

Fig. 12. Location (a) and seismic profile (b) of a Carboniferous intra-arc volcanic basin in the Luliang area (after Yang et al., 2012a).

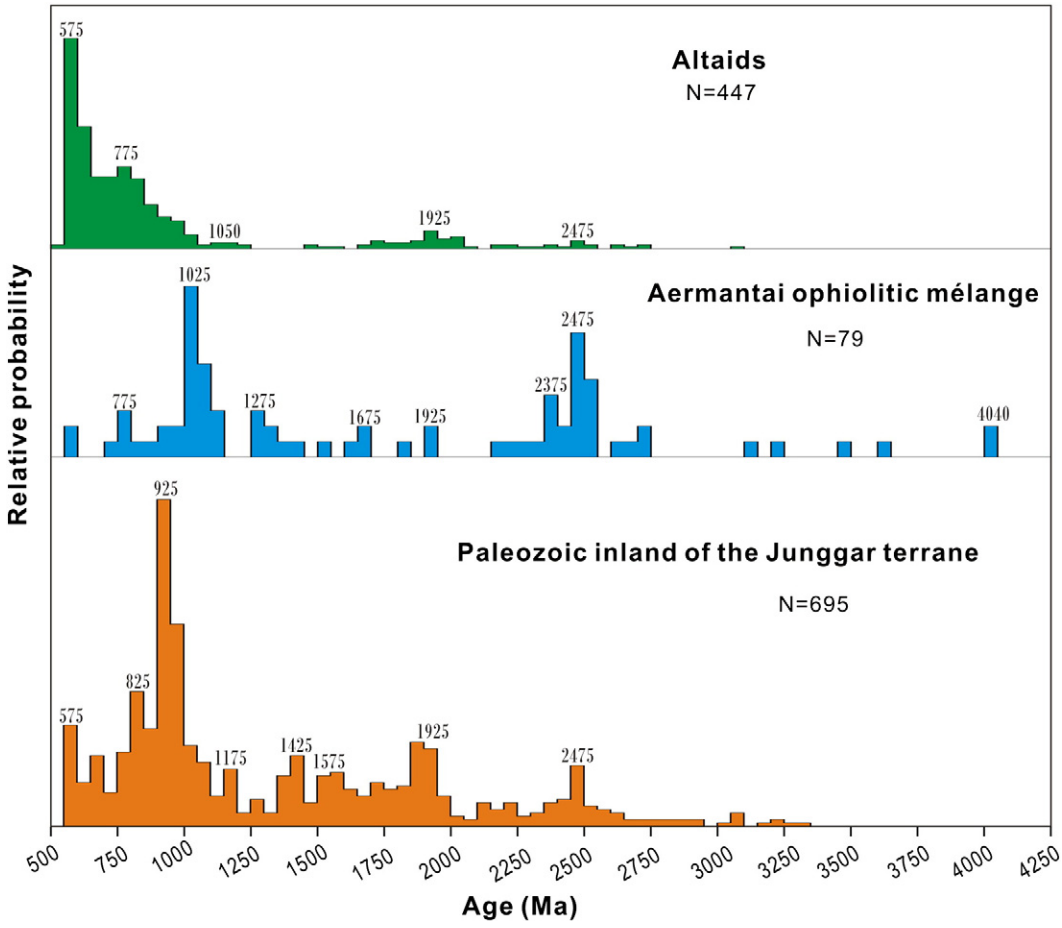

Fig. 13. Relative U–Pb age probability for the Precambrian detrital zircons from the Aermantai ophiolitic mélange and within the Junggar terrane. The data for the Aermantai ophiolitic mélange are from Huang et al. (2013), the data for the Altai Orogen are from Long et al. (2007), Sun et al. (2008) and Jiang et al. (2011), and the data for Paleozoic inland of the Junggar terrane are from this study, Chen et al (2009), He et al. (2012b), Huang et al. (2014), Hu et al (2006, 2010), Lei et al (2011), Li et al (2007), Q.G. Li et al. (2009), Long et al (2012), Ma et al (2012), Su et al (2008) and Xu et al. (2013).

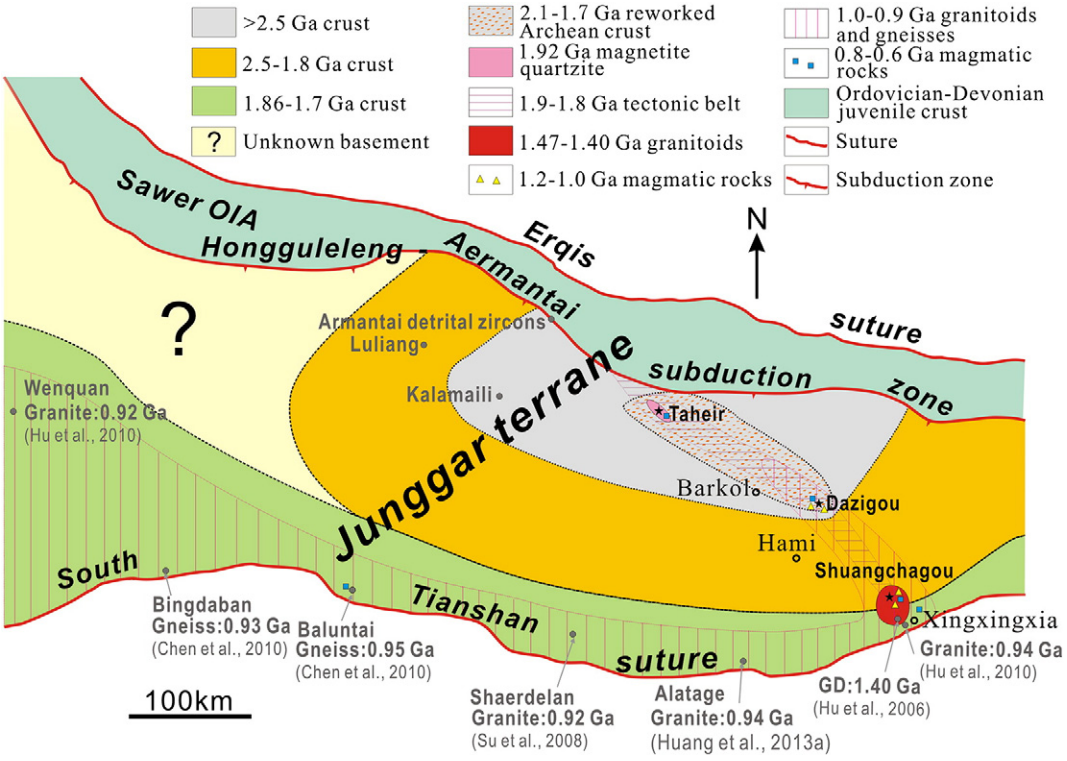

Fig. 14. An outline of the crust basement of the Junggar terrane. The boundary lines of the different basement, tectonic and magmatic belts, and quartzite formation of the Junggar terrane are inferred. GD: granodiorite; OIA: oceanic island arc. Gray dots show the sample locations of the published data. Black stars show the sample locations of this study.

exhibited by 1.88 Ga dioritic gneiss in the Taheir area and 1.9–1.8 Ga magmatic events in the Taheir, Dazigou and Shuangchagou area that possibly present along the Taheir–Dazigou–Shuangchagou line. There is a massive 1.0–0.9 Ga magmatic–metamorphic belt along the Tianshan range and Shuangchagou–Dazigou area, 1.47–1.40 Ga granitoids in the Shuangchagou–Xingxingxia area, 1.2–1.0 Ga magmatic rocks in the Dazigou–Shuangchagou area, and 0.8–0.6 Ga magmatic rocks in the Taheir, Dazigou, Shuangchagou and Baluntai area.

6.2. Origin of the Precambrian Junggar terrane

6.2.1. Relation of the Precambrian Junggar terrane to adjacent terrane and cratons

According to the suggestion that both the Erqis ocean and South Tianshan ocean were opened before the Ordovician and closed during the Carboniferous–Early Permian (e.g. Gao et al., 2009; Xiao et al., 2009a; Biske and Seltmann, 2010; Han et al., 2010; Wong et al., 2010; Gao et al., 2011; Glorie et al., 2011; Han et al., 2011; Long et al., 2011; Liu et al., 2012; Su et al., 2012; Xu et al., 2013; Li et al., 2014), the detrital zircons from the Ordovician metasedimentary rock in the Baluntai area, Ordovician graywackes near the Dazigou area, Late Silurian sedimentary sequences in the Aermantai ophiolitic mélange and Devonian sandstones in the Kalamaili area should have originated from the Paleozoic inland location of the Junggar terrane; therefore, they could have participated in the reconstruction of tectonic evolution process of the Junggar terrane. On the basis of the new zircon U–Pb age data of this study and a large quantity of published zircon U–Pb age data for the Junggar terrane, the age spectra of Precambrian zircons from the Junggar terrane have more similar age peaks with the neighboring Mongolia terranes than the Tarim craton, Southern Siberian, North China craton and Northeastern Gondwana (Fig. 15). The Junggar terrane, Mongolia terrane, Tarim craton, Northeastern Gondwana Southern Siberian and North China craton all have similar age peaks of 2575 or 2525 or 2475 Ma, and 1875 or 1825 Ma, indicating that they all contain an Archean basement and 1.9–1.8 Ga orogens, along which the supercontinent Columbia was assembled (Zhao et al., 2002). However, the Junggar terrane and Mongolia terrane are dominated by zircons in the age range of 1500–550 Ma, and zircons in that age range do not exist in the age spectra of the Tarim craton, southern Siberian craton and North China craton (Rojas-Agramonte et al., 2011; He et al., 2012a; Ma et al., 2012; Z.Y. He et al., 2013), implying that the Junggar terrane and Mongolia terrane were most likely not derived from the Tarim craton, southern Siberian craton and North China craton (He et al., 2012b). The scarcity of 1100–1500 Ma zircons and tectonism in Northeastern Gondwana means that they are not related to the Northeastern Gondwana as well. The occurrence of the similar age peaks of 2475 Ma, 1725 Ma, 1425 or 1375 Ma and 1125 or 1175 Ma, and 925 Ma in the spectra of the Junggar terrane and Mongolia terrane indicate that the two terranes have a similar tectonism and origin.

6.2.2. Origin of the Precambrian Junggar terrane

The occurrence of a great number of 1.8–1.3 Ga zircons in the Precambrian Junggar terrane relate the Precambrian Junggar terrane to the 1.8–1.3 Ga magmatic accretion of the supercontinent Columbia along the present-day southern margin of North America, Greenland and Baltica and the western margin of South America (Zhao et al., 2004). The coexistence of the distinctive 1.92 Ga magnetite quartzite, 1.9–1.8 Ga orogen and 1.47–1.40 Ga granitoids in the Precambrian Junggar terrane indicates that the Precambrian Junggar terrane possibly split from southern Laurentia near the Lake Superior region because the ~1.40 Ga granitoids are mainly present in southern Laurentia and there is a coexistence of 1.9–1.8 Ga orogen and 2.1–1.9 Ga quartzite, which are restricted to the Lake Superior region (Nyman et al., 1994; Kirby et al., 1995; Thompson et al., 1996; Ojakangas et al., 2001; Crowley et al., 2006; Goodge and Vervoort, 2006; Whitmeyer and Karlstrom, 2013). The occurrence of 4.0 Ga zircons and material in the Junggar terrane also relates the Precambrian Junggar terrane to the Laurentia continent because the development of the 4.0 Ga crust was unique to the Slave

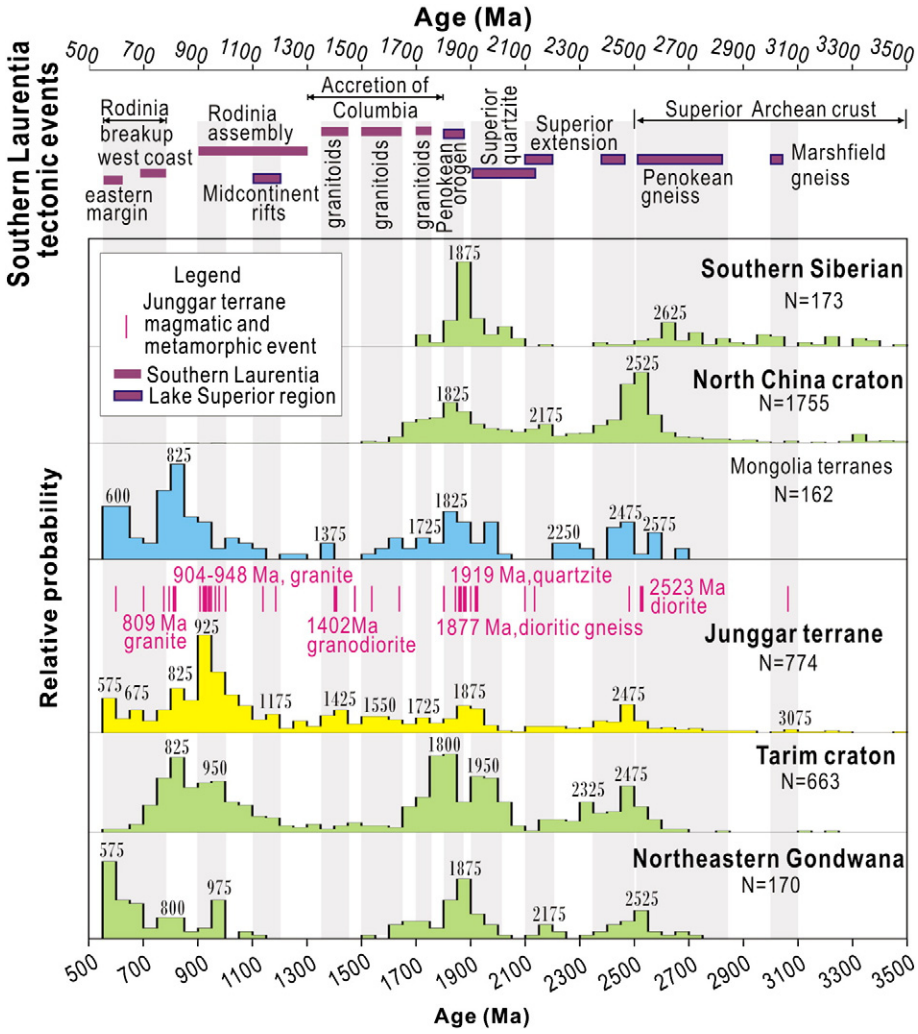

Fig. 15. Relative U–Pb age probability for the Precambrian zircons from the Junggar terrane, Tarim craton, Mongolia terrane, North China craton, northeastern Gondwana and southern Siberian craton with a comparison to the tectonism of southern Laurentia. The data for Mongolia terrane, North China craton, Northeastern Gondwana and Southern Siberian are from Rojas-Agramonte et al (2011), the data for Tarim craton are from C.L. Zhang et al. (2007, 2009), Shu et al. (2011), He et al. (2012a), Z.Y. He et al. (2013) and Dong et al (2012). The data from the Aermantai ophiolitic mélange (Huang et al., 2013) is combined to the data source for the Junggar terrane. Epoch of tectonism of southern Laurentia is from Karlstrom et al (2001), Zhao et al (2004) and Whitmeyer and Karlstrom (2013).

craton in the Laurentia continent (Bowring et al., 1989; Bowring and Housh, 1995; Stern and Bleeker, 1998; Bowring and Williams, 1999; Iizuka et al., 2006; Pietranik et al., 2008). Similar ~4.0 Ga zircons were discovered in the Wyoming craton west of the Lake Superior craton (Houston, 1993; Mueller et al., 1992). This genetic hypothesis is also supported by the following evidence: 1) the Precambrian Junggar terrane has a similar >3.0 Ga crust and 2.52 Ga intrusions as the Lake Superior craton (Sims et al., 1989); 2) Taheir Archean crust was reworked at approximately 2.1–1.7 Ga, which is similar to the reworking of the Lake Superior Archean crust along the Trans Hudson Orogen at 1.9–1.8 Ga; 3) 2.45 Ga, 2.2–2.1Ga, and 1.2–1.1 Ga magmatism of the Precambrian Junggar terrane are perfectly correlated to the tectonism of the two-stage extension and midcontinent rifting in the Lake Superior region (Whitmeyer and Karlstrom, 2013); and 4) eastward extensions of both the Penokean orogen and Animikie basin are truncated by the Grenville Orogen (Hoffman, 1988), and the Precambrian Junggar terrane was possibly a lost segment of the east Animikie basin and Penokean orogen. The Taheir–Dazigou Archean crust was possibly adjacent to the Lake Superior craton, whereas the Shuangchagou–Luliang 2.5–1.8 Ga crust was possibly the east-extension of the 2.0–1.8 Ga Pembine–Wausau arc, and Central Tianshan was possibly related to the Yavapai Province (Whitmeyer and Karlstrom, 2013). The occurrence of a 1.2–1.0 Ga magmatic zircon population that correlates to midcontinent rifting indicates a split of the Precambrian Junggar terrane from the Lake Superior region that is possibly related to midcontinent rifting at 1.2–1.0 Ga. Abundant 1.0–0.90 Ga granitoids and gneiss as well as 0.8–0.6 Ga magmatism indicate that the Junggar split possibly moved to the Caborca region, which is located at an intersection between the final collision belt for the Rodinia assembly along the southern margin of Laurentia and the breakup line for Rodinia along the western margin of Laurentia. Evidence that the 0.8–0.6 Ga magmatic zircons and rocks are mainly present in the Taheir, Dazigou and Shuangchagou area and present in the east Junggar terrane indicates that the Precambrian Junggar terrane was possibly turned, which resulted in the Tianshan region facing southern Laurentia and the presence of 0.8–0.6 Ga magmatic rocks in the Taheir–Dazigou–Shuangchagou area at the northwestern part of the 1.0–0.6 Ga Junggar terrane.

However, the context of the three crust basement units and Precambrian tectonic–magmatic–metamorphic belts of the Precambrian Junggar terrane must be precisely constrained in the future, and the relationship between the Precambrian Junggar terrane and southern Laurentia must be made clear.

7. Conclusion

The Junggar terrane has three Precambrian basement units, including the Taheir–Kalamaili–Dazigou Archean crust that formed at approximately 3.2–3.0 Ga and includes 2.52 Ga diorites and 4.0 Ga zircons and materials; the Shuangchagou–Luliang crust that formed at approximately 2.5–1.8 Ga crust; and the Tianshan crust that formed at approximately 1.86–1.7 Ga between the Hongguleleng–Aermantai subduction zone and the south Tianshan suture. The Taheir Archean crust was reworked at approximately 2.1–1.7 Ga. In addition, the following possibly exist: a 1.92 Ga quartzite formation in the Taheir area, a 1.9–1.8 Ga orogen along the Taheir–Dazigou–Shuangchagou line, 1.47–1.40 Ga granitoids in the Shuangchagou–Xingxingxia area, 1.2–1.0 Ga magmatic rocks in the Dazigou–Shuangchagou area, a massive 1.0–0.9 Ga magmatic–metamorphic rock belt along the Tianshan range and Shuangchagou–Dazigou area, and 0.8–0.6 Ga magmatic rocks in the Taheir, Dazigou, Shuangchagou and Baluntai areas. Regular arrangements of the three basement units and various sedimentary, magmatic and metamorphic belts possibly relate the Precambrian Junggar terrane to southern Laurentia near the Lake Superior region before 1.1 Ga and to the area adjacent to the Caborca region at 1.0–0.6 Ga as a split.

Acknowledgments

This research was supported by the National Natural Science Foundation of China (grant numbers 41390422 and 41072060), CAS Knowledge Innovation Project (grant numbers kzcx-ew-ly03 and kzcx2-yw-107) and National 305 project (grant numbers 2011BAB06B03-3 and 2006BAB07B01-03). We are indebted to Yu Liu and Guoqiang Tang for their help in conducting the Cameca IMS-1280 ion microprobe, Xin Yan and Saihong Yang for their assistance with SEM analyses, and Qi Wu, Jun You, Tao Hong and Peng Xiang for their field assistance. We thank Wenjiao Xiao, Kezhang Qin, JinHui Guo, GuoQi He and Guangmin Li for their valuable discussions. This paper was significantly improved by the thorough and incisive review of Wenjiao Xiao, Zeming Zhang, Guochun Zhao, and two anonymous reviewers.

Appendix A. Supplementary data

Supplementary tables to this article can be found online at http://dx.doi.org/10.1016/j.gr.2014.03.011.

References

Albarède, F., 2003. Geochemistry: An Introduction. Cambridge University Press p. 248.
Allen, M.B., Vincent, S.J., 1997. Fault reactivation in the Junggar region, northwest China: the role of basement structures during Mesozoic–Cenozoic compression. Journal of the Geological Society, London 154, 151–155.
Allen, M.B., Windley, B.F., Zhang, C., 1992. Palaeozoic collisional tectonics and magmatism of the Chinese Tien Shan, central Asia. Tectonophysics 220, 89–115.
Amelin, Y., Lee, D.C., Halliday, A.N., Pidgeon, R.T., 1999. Nature of the Earth's earliest crust from hafnium isotopes in single detrital zircons. Nature 399, 252–255.
Ao, S.J., Xiao, W.J., Han, C.M., Li, X.H., Qu, J.F., Zhang, J.E., Guo, Q.Q., Tian, Z.H., 2012. Cambrian to early Silurian ophiolite and accretionary processes in the Beishan collage, NW China: implications for the architecture of the Southern Altaids. Geological Magazine 149, 606–625.
Badarch, G., Cunningham, W.D., Windley, B.F., 2002. A new terrane subdivision for Mongolia: implications for the Phanerozoic crustal growth of Central Asia. Journal of Asian Earth Sciences 21, 87–110.
Bailey, J.C., 1981. Geochemical criteria for a refined tectonic discrimination of orogenic andesites. Chemical Geology 32, 139–154.
Bailey, J.C., Frolova, T.I., Burikova, I.A., 1989. Mineralogy, geochemistry and petrogenesis of Kurile island-arc basalts. Contributions to Mineralogy and Petrology 102, 265–280.
Bazhenov, M.L., Levashova, N.M., Degtyarev, K.E., Van der Voo, R., Abrajevitch, A.V., McCausland, P.J.A., 2012. Unraveling the early–middle Paleozoic paleogeography of Kazakhstan on the basis of Ordovician and Devonian paleomagnetic results. Gondwana Research 22, 974–991.
Best, M.G., Christiansen, E.H., 2001. Igneous Petrology. Blackwell Science p. 458.
Biske, Yu.S., Seltmann, R., 2010. Paleozoic Tian-Shan as a transitional region between the Rheic and Urals–Turkestan oceans. Gondwana Research 17, 602–613.
Bodet, F., Scharer, U., 2000. Evolution of the SE-Asian continent from U–Pb and Hf isotopes in single grains of zircon and baddeleyite from large rivers. Geochimica et Cosmochimica Acta 64, 2067–2091.
Bowring, S.A., Housh, T., 1995. The Earth's early evolution. Science 269, 1535–1540.
Bowring, S.A., Williams, I.S., 1999. Priscoan (4.00–4.03 Ga) orthogneisses from northwestern Canada. Contributions to Mineralogy and Petrology 134, 3–16.
Bowring, S.A., Williams, I.S., Compston, W., 1989. 3.96 Ga gneisses from the Slave province, Northwest Territories, Canada. Geology 17, 971–975.
Buchan, C., Pfänder, J., Kröner, A., Brewer, T.S., Tomurtogoo, O., Tomurhuu, D., Cunningham, D., Windley, B.F., 2002. Timing of accretion and collisional deformation in the Central Asian Orogenic Belt: implications of granite geochronology in the Bayankhongor Ophiolite Zone. Chemical Geology 192, 23–45.
Buslov, M.M., Fujiwara, Y., Iwata, K., Semakov, N.N., 2004. Late Paleozoic–Early Mesozoic geodynamics of Central Asia. Gondwana Research 7, 791–808.
Carroll, A.R., Liang, Y., Graham, S.M., Xiao, X., Hendrix, M.S., Chu, J., McKnight, C.L., 1990. Junggar basin, northwest China: trapped Late Paleozoic ocean. Tectonophysics 181, 1–14.
Charvet, J., Laurent-Charvet', S., Shu, L., Ma, R., 2001. Paleozoic continental accretions in Central Asia around Junggar block: new structural and geochronological data. Gondwana Research 4, 590–592.
Charvet, J., Shu, S.L., Laurent-Charvet, S., 2007. Paleozoic structural and geodynamic evolution of eastern Tianshan (NW China): welding of the Tarim and Junggar plates. Episodes 30, 162–186.
Chen, B., Jahn, B.M., 2004. Genesis of post-collisional granitoids and basement nature of the Junggar Terrane, NW China: Nd–Sr isotope and trace element evidence. Journal of Asian Earth Sciences 23, 691–703.
Chen, C., Lua, H., Jia, D., Cai, D., Wu, S., 1999. Closing history of the southern Tianshan oceanic basin, western China: an oblique collisional orogeny. Tectonophysics 302, 23–40.
Chen, X.Y., Wang, Y.J., Sun, L.H., Fan, W.M., 2009. Zircon SHRIMP U–Pb dating of the granitic gneisses from Bingdaban and Laerdundaban (Tianshan Orogen) and their geological significances. Geochimica 38, 424–431 (in Chinese with English abstract).
Chen, R.X., Zheng, Y.F., Xie, L.W., 2010. Metamorphic growth and recrystallization of zircon: distinction by simultaneous in-situ analyses of trace elements, U–Th–Pb and Lu–Hf isotopes in zircons from eclogite–facies rocks in the Sulu orogen. Lithos 114, 132–154.
Chiaradia, M., Fontboté, L., Beate, B., 2004. Cenozoic continental arc magmatism and associated mineralization in Ecuador. Mineralium Deposita 39, 204–222.
Choulet, F., Faure, M., Cluzel, D., Chen, Y., Lin, W., Wang, B., 2012. From oblique accretion to transpression in the evolution of the Altaid collage: new insights from West Junggar, northwestern China. Gondwana Research 21, 530–547.
Coleman, R.G., 1989. Continental growth of northwest China. Tectonics 8, 621–635.
Condie, K.C., 1999. Mafic crustal xenoliths and the origin of the lower continental crust. Lithos 46, 95–101.
Condie, K.C., 2000. Episodic continental growth models: afterthoughts and extensions. Tectonophysics 322, 153–162.
Corfu, F., Hanchar, J.M., Hoskin, P.W.O., Kinny, P., 2003. Atlas of zircon textures. Reviews in Mineralogy and Geochemistry 53, 469–500.
Crowley, J.L., Schmitz, M.D., Bowring, S.A., Williams, M.L., Karlstrom, K.E., 2006. U–Pb and Hf isotopic analysis of zircon in lower crustal xenoliths from the Navajo volcanic field: 1.4 Ga mafic magmatism and metamorphism beneath the Colorado Plateau. Contributions to Mineralogy and Petrology 151, 313–330.
Dhuime, B., Hawkesworth, C.J., Cawood, P.A., Storey, C.D., 2012. A change in the geodynamics of continental growth 3 billion years ago. Science 335, 1334–1336.
Dobretsov, N.L., Buslov, M.M., Vernikovsky, V.A., 2003. Neoproterosoic to Early Ordovocian evolution of the Paleo-Asian Ocean: implications to the break-up of Rodinia. Gondwana Research 6, 143–159.
Dong, L.H., Xu, X.W., Qu, X., Li, G.M., 2009. Tectonic setting and formation mechanism of the circum-Junggar porphyritic copper deposit belts. Acta Petrologica Sinica 25, 713–717 (in Chinese with English abstract).
Dong, L.H., Xu, X.W., Zhao, S.M., 2012. Discovery and significance of 1.95 Ga BIF in the Kuluketage area, Xinjiang. Xinjiang Geology 30, 371–376 (in Chinese with English abstract).
Du, S.J., Qu, X., Deng, G., Zhang, Y., Cheng, S.L., Lu, H.F., Wu, Q., Xu, X.W., 2010. Chronology and tectonic setting of intrusive bodies and associated porphyry copper deposit in the Hersai area, Eastern Junggar. Acta Petrologica Sinica 26, 2981–2996 (in Chinese with English abstract).
Ellam, R.M., Hawkesworth, C.J., 1988. Elemental and isotopic variations in subduction related basalts: evidence for a three component model. Contributions to Mineralogy and Petrology 98, 72–80.
Filippova, I.B., Bush, V.A., Didenko, A.N., 2001. Middle Paleozoic subduction belts: the leading factor in the formation of the Central Asian fold-and-thrust belt. Russian Journal of Earth Sciences 3, 405–426.
Gao, J., Li, M.S., Xiao, X.C., Tang, Y.Q., He, G.Q., 1998. Paleozoic tectonic evolution of the Tianshan orogen, northwestern China. Tectonophysics 287, 213–231.
Gao, J., Long, L.L., Klemd, R., Qian, Q., Liu, D.Y., Xiong, X.M., Su, W., Liu, W., Wang, Y.T., Yang, F.Q., 2009. Tectonic evolution of the South Tianshan orogen and adjacent regions, NW China: geochemical and age constraints of granitoid rocks. International Journal of Earth Sciences 98, 1221–1238.
Gao, J., Klemd, R., Qian, Q., Zhang, X., Li, J.L., 2011. The collision between the Yili and Tarim blocks of the Southwestern Altaids: geochemical and age constraints of a leucogranite dike crosscutting the HP–LT metamorphic belt in the Chinese Tianshan Orogen. Tectonophysics 499, 118–131.
Gärtner, A., Linnemann, U., Sagawe, A., Hofmann, M., Ullrich, B., Kleber, A., 2013. Morphology of zircon crystal grains in sediments—characteristics, classifications, definitions. Journal of Central European Geology 59, 65–73.

Glorie, S., De Grave, J., Buslov, M.M., Zhimulev, F.I., Izmer, A., Vandoorne, W., Ryabinin, A., Van den haute, P., Vanhaecke, F., Elburg, M.A., 2011. Formation and Palaeozoic evolution of the Gorny-Altai–Altai-Mongolia suture zone (South Siberia): Zircon U/Pb constraints on the igneous record. Gondwana Research 20, 465–484.

Goodge, J.W., Vervoort, J.D., 2006. Origin of Mesoproterozoic A-type granites in Laurentia: Hf isotope evidence. Earth and Planetary Science Letters 243, 711–731.

Goolaerts, A., Mattielli, N., de Jong, J., Weis, D., Scoates, J.S., 2004. Hf and Lu isotopic reference values for the zircon standard 91500 by MC–ICP–MS. Chemical Geology 206, 1–9.

Goss, A.R., Kay, S.M., Mpodozis, C., 2011. The geochemistry of a dying continental arc: the In capillo Caldera and Dome Complex of the southernmost Central Andean Volcanic Zone (~28°S). Contributions to Mineralogy and Petrology 161, 101–128.

Greene, A.R., DeBari, S.M., Kelemen, P.B., Blusztajn, J., Clift, P.D., 2006. A detailed geochemical study of island arc crust: the Talkeetna Arc section, south-central Alaska. Journal of Petrology 47, 1051–1093.

Griffin, W.L., Belousova, E.A., Shee, S.R., Pearson, N.J., O'Reilly, S.Y., 2004. Archean crustal evolution in the northern Yilgarn Craton: U–Pb and Hf-isotope evidence from detrital zircons. Precambrian Research 131, 231–282.

Han, B.F., Guo, Z.J., Zhang, Z.C., Zhang, L., Chen, J.F., Song, B., 2010. Age, geochemistry, and tectonic implications of a late Paleozoic stitching pluton in the North Tian Shan suture zone, western China. Geological Society of America Bulletin 122, 627–640.

Han, B.F., He, G.Q., Wang, X.C., Guo, Z.J., 2011. Late Carboniferous collision between the Tarim and Kazakhstan–Yili terranes in the western segment of the South Tian Shan Orogen, Central Asia, and implications for the Northern Xinjiang, western China. Earth-Science Reviews 109, 74–93.

He, G.Q., Li, M.S., Liu, D.Q., Zhou, N.H., 1994. Palaeozoic crustal evolution and mineralization in Xinjiang of China. Xinjiang People's Publication House, Urumqi p. 437 (in Chinese with English abstract).

He, Z.Y., Zhang, Z.M., Zong, K.Q., Wang, W., Santoshd, M., 2012a. Neoproterozoic granulites from the northeastern margin of the Tarim Craton: petrology, zircon U–Pb ages and implications for the Rodinia assembly. Precambrian Research 212–213, 21–33.

He, Z.Y., Zhang, Z.M., Zong, K.Q., Yu, F., Wang, W., 2012b. Zircon geochronology of Xingxingxia quartz dioritic gneisses: implications for the tectonic evolution and Precambrian basement affinity of Chinese Tianshan orogenic belt. Acta Petrologica Sinica 28, 1857–1874.

He, D.F., Li, D., Fan, C., Yang, X.F., 2013a. Geochronology, geochemistry and tectonostratigraphy of Carboniferous strata of the deepest Well Moshen in the Junggar Basin, Northwest China: insights into the continental growth of Central Asia. Gondwana Research 24, 560–577.

He, Z.Y., Zhang, Z.M., Zong, K.Q., Dong, X., 2013b. Paleoproterozoic crustal evolution of the Tarim Craton: constrained by zircon U–Pb and Hf isotopes of meta-igneous rocks from Korla and Dunhuang. Journal of Asian Earth Sciences 78, 54–70.

Hoffman, P.F., 1988. United plates of America, the birth of a craton; early Proterozoic assembly and growth of Laurentia. Annual Review of Earth and Planetary Sciences 16, 543–603.

Hofmann, A.W., 1988. Chemical differentiation of the Earth: the relationship between mantle, continental crust, and oceanic crust. Earth and Planetary Science Letters 90, 297–314.

Hoskin, P.W.O., Black, L.P., 2000. Metamorphic zircon formation by solid-state recrystallization of protolith igneous zircon. Journal of Metamorphic Geology 18, 423–439.

Houston, R.S., 1993. Late Archean and Early Proterozoic geology of the Wyoming province. In: Snoke, A.W., Steidtmann, J.R. (Eds.), Geology of Wyoming. Geological Survey of Wyoming Memoir, 5, pp. 78–116.

Hu, A.Q., Jahn, B.M., Zhang, G.X., Chen, Y.B., Zhang, Q.F., 2000. Crustal evolution and Phanerozoic crustal growth in northern Xinjiang: Nd isotopic evidence: Part I. Isotopic characterization of basement rocks. Tectonophysics 328, 15–51.

Hu, A.Q., Wei, G.J., Deng, W.F., Zhang, J.B., Chen, L.L., 2006. 1.4 Ga SHRIMP U–Pb age for zircons of granodiorite and its geological significance from the eastern segment of the Tianshan Mountains, Xinjiang, China. Geochimica 35, 333–345 (in Chinese with English abstract).

Hu, A.Q., Wei, G.J., Jahn, B.M., Zhang, J.B., Deng, W.F., Chen, L.L., 2010. Formation of the 0.9 Ga Neoproterozoic granitoids in the Tianshan Orogen, NW China: constraints from the SHRIMP zircon age determination and its tectonic significance. Geochimica 39, 197–212 (in Chinese with English abstract).

Huang, G., Niu, G.Z., Zhang, Z.W., Wang, X.L., Xu, X.Y., Guo, J., Yu, F., 2013. Discovery of ~4.0 Ga detrital zircons in the Aermantai ophiolitic mélange, East Junggar, northwest China. Chinese Science Bulletin 58, 3645–3663.

Huang, B.T., He, Z.Y., Zong, K.Q., Zhang, Z.M., 2014. Zircon U–Pb and Hf isotopic study of Neoproterozoic granitic gneisses from the Alatage area, Xinjiang: constraints on the Precambrian crustal evolution in the Central Tianshan Block. Chinese Science Bulletin 59, 100–112.

Iizuka, T., McCulloch, M.T., Komiya, T., Shibuya, T., Ohta, K., Ozawa, H., Sugimura, E., Windley, B.F., 2006. 4.2 Ga zircon xenocryst in an Acasta gneiss from northwestern Canada: evidence for early continental crust. Geology 34, 245–248.

Jahn, B.M., Wu, F., Lo, C.H., Tsai, C.H., 1999. Crust–mantle interaction induced by deep subduction of the continental crust: geochemical and Sr–Nd isotopic evidence from post-collisional mafic–ultramafic intrusions of the northern Dabie complex, central China. Chemical Geology 157, 119–146.

Jahn, B.M., Wu, F., Chen, B., 2000. Granitoids of the Central Asian Orogenic Belt and continental growth in the Phanerozoic. Transactions of the Royal Society of Edinburgh: Earth Sciences 91, 181–193.

Jahn, B.M., Capdevila, R., Liu, D., Vernon, A., Badarch, G., 2004. Sources of Phanerozoic granitoids in the transect Bayanhongor–Ulaan Baatar, Mongolia: geochemical and Nd isotopic evidence, and implications for Phanerozoic crustal growth. Journal of Asian Earth Sciences 23, 629–653.

James, H.L., 1954. Sedimentary facies of iron formation. Economic Geology 49, 235–293.

Jian, P., Liu, D.Y., Zhang, Q., Zhang, F.Q., Shi, Y.R., Shi, G.H., Zhang, L.Q., Tao, H., 2003. SHRIMP dating of ophiolite and leucocratic rocks within ophiolite. Earth Science Frontier 10, 439–456 (in Chinese with English abstract).

Jian, P., Liu, D.Y., Shi, Y.R., Zhang, F.Q., 2005. SHRIMP dating of SSZ ophiolites from northern Xinjiang Province, China: implications for generation of oceanic crust in the Central Asian Orogenic Belt. In: Sklyarov, E.V. (Ed.), Structural and tectonic correlation across the Central Asia Orogenic Collage: North-Eastern Segment. Guidebook and Abstract Volume of the SiberianWorkshop IGCP-480. IEC SB RAS, Irkutsk, p. 246.

Jiang, Y., Sun, M., Zhao, G., Yuan, C., Xiao, W., Xia, X., Long, X., Wu, F., 2011. Precambrian detrital zircons in the Early Paleozoic Chinese Altai: their provenance and implications for the crustal growth of central Asia. Precambrian Research 189, 140–154.

Jiang, N., Chen, J., Guo, J., Chang, G., 2012. In situ zircon U–Pb, oxygen and hafnium isotopic compositions of Jurassic granites from the North China craton: evidence for Triassic subduction of continental crust and subsequent metamorphism-related ^{18}O depletion. Lithos 142–143, 84–94.

Karlstrom, K.E., Ahall, K.-I., Harlan, S.S., William, M.L., McLelland, J., Geissman, J.W., 2001. Long-lived (1.8–0.8 Ga) convergent orogen in southern Laurentia, its extensions to Australia and Baltica, and implications for refining Rodinia. Precambrian Research 111, 5–30.

Keller, R.A., Fisk, M.R., Smellie, J.L., Strelin, J.A., Lawver, L.A., 2002. Geochemistry of back arc basin volcanism in Bransfield Strait, Antarctica: subducted contributions and along-axis variations. Journal of Geophysical Research 107, B8. http://dx.doi.org/10.1029/2001JB000444.

Kirby, E., Karlstrom, K.E., Andronicos, C.L., Dallmeyer, C.L., R.D., 1995. Tectonic setting of the Sandia pluton—An orogenic 1.4 Ga granite in New Mexico. Tectonics 14, 185–201.

Koloskov, A.V., Flerov, G.B., Perepelov, A.B., Melekestsev, I.V., Puzankov, M.Yu., Filosofova, T.M., 2011. Evolution stages and petrology of the Kekuknai Volcanic Massif as reflecting the magmatism in Backarc Zone of Kuril–Kamchatka Island Arc System. Part 1. Geological position and geochemistry of volcanic rocks. Journal of Volcanology and Seismology 5, 312–334.

Kröner, A., Windley, B.F., Badarch, G., Tomurtogoo, O., Hegner, E., Liu, D.Y., Wingate, M.T.D., 2007. Accretionary growth and crust formation in the Central Asian Orogenic Belt and comparison with the Arabian–Nubian shield. In: Hatcher Jr., R.D., Carlson, M.P., McBride, J.H., Martínez Catalán, J.R. (Eds.), 4-D framework of continental crust. Geological Society of America Memoir, 200, pp. 181–209.

Kwon, S.T., Tiltong, G.R., Coleman, R.G., Feng, Y., 1989. Isotopic studies bearing on the tectonics of the west Junggar region. Xinjiang, China. Tectonics 8, 719–727.

Le Bas, M.J., Le Maitre, R.W., Streckeisen, A., Zanettin, B., 1986. A chemical classification of volcanic rocks based on the total alkalisilica diagram. Journal of Petrology 27, 745–750.

Le Roux, A.P., 1986. Geochemical correlation between southern African kimberlites and south Atlantic hotspots. Nature 324, 243–245.

Lei, R.X., Wu, C.Z., Gu, L.X., Zhang, Z.Z., Chi, G.X., Jiang, Y.H., 2011. Zircon U–Pb chronology and Hf isotope of the Xingxingxia granodiorite from the Central Tianshan zone (NW China): implications for the tectonic evolution of the southern Altaids. Gondwana Research 20, 582–593.

Li, J.Y., Xiao, X.C., Chen, W., 2000. Late Ordovician continental basement of the eastern Junggar Basin in Xinjiang, NW China: evidence from the Laojunmiao metamorphic complex on the northeast basin margin. Xinjiang Geology 19, 297–302 (in Chinese with English abstract).

Li, Y.P., Li, J.Y., Sun, G.H., Zhu, Z.X., Yang, Z.Q., 2007. Basement of Junggar basin: evidence from detrital zircons in sandstone of previous Devonian Kalamaili formation. Acta Petrologica Sinica 23, 1577–1590 (in Chinese with English abstract).

Li, Q.G., Liu, S.W., Song, B., Wang, Y.B., Chen, Y.Z., 2009. Late Mesoproterozoic to Paleozoic tectonothermal events in the Eastern Segment of the Central Tianshan tectonic zone of Northwestern China: constraints from SHRIMP zircon geochronology. Earth Science Frontiers 16, 175–184 (in Chinese with English abstract).

Li, X.H., Liu, Y., Li, Q.L., Guo, C.H., Chamberlain, K.R., 2009. Precise determination of Phanerozoic zircon Pb/Pb age by multi-collector SIMS without external standardization. Geochemistry Geophysics Geosystem 10, Q04010. http://dx.doi.org/10.1029/2009GC002400.

Li, Q.L., Li, X.H., Liu, Y., Tang, G.Q., Yang, J.H., Zhu, W.G., 2010. Precise U–Pb and Pb–Pb dating of Phanerozoic baddeleyite by SIMS with oxygen flooding technique. Journal of Analytical Atomic Spectrometry 25, 1107–1113.

Li, X.H., Tang, G.Q., Guo, B., Yang, Y.H., Hou, K.J., Hu, Z.C., L Q.L., Liu, Y., Li, W.X., 2013. Qinghu zircon: a working reference for microbeam analysis of U–Pb age and Hf and O isotopes. Chinese Science Bulletin 58, 1954–1961 (in Chinese).

Li, D., He, D.F., Santosh, M., Tang, J.Y., 2014. Petrogenesis of Late Paleozoic volcanics from the Zhaheba depression, East Junggar: insights into collisional event in an accretionary orogen of Central Asia. Lithos 184–187, 167–193.

Lin, J.F., Yu, H.X., Yu, X.Q., Di, Y.J., Tian, J.T., 2007. Zircon SHRIMP U–Pb dating and geological implication of the Sabei alkali-rich granite from Eastern Junggar of Xinjiang, NW China. Acta Petrologica Sinica 23, 1876–1884 (in Chinese with English abstract).

Liu, W., Liu, X.J., Xiao, W.J., 2012. Massive granitoid production without massive continental-crust growth in the Chinese Altay: insight into the source rock of granitoids using integrated zircon U–Pb age, Hf–Nd–Sr isotopes and geochemistry. American Journal of Science 312, 629–684.

Long, X.P., Sun, M., Yuan, C., Xiao, W.J., Lin, S., Wu, F.Y., Xia, X.P., Cai, K.D., 2007. Detrital zircon age and Hf isotopic studies for metasedimentary rocks from the Chinese Altai: implications for the Early Paleozoic tectonic evolution of the Central Asian Orogenic Belt. Tectonics 26, TC5015. http://dx.doi.org/10.1029/2007TC002128.

Long, L.L., Gao, J., Klemd, R., Beier, C., Qian, Q., Zhang, X., Wang, J.B., Jiang, T., 2011. Geochemical and geochronological studies of granitoid rocks from the Western Tianshan Orogen: implications for continental growth in the southwestern Central Asian Orogenic Belt. Lithos 126, 321–340.

Long, X., Yuan, C., Sun, M., Safonova, I., Xiao, W., Wang, Y., 2012. Geochemistry and U–Pb detrital zircon dating of Paleozoic graywackes in East Junggar, NW China: insights into subduction–accretion processes in the southern Central Asian Orogenic Belt. Gondwana Research 21, 637–653.
Ludwig, K.R., 2001. Users' manual for Isoplot/Ex rev. 2.49. Berkeley Geochronology Centre Special Publication. No. 1a.
Ma, X.X., Shu, L.S., Santosh, M., Li, J.Y., 2012. Detrital zircon U–Pb geochronology and Hf isotope data from Central Tianshan suggesting a link with the Tarim Block: implications on Proterozoic supercontinent history. Precambrian Research 206–207, 1–16.
Martynov, A., Khanchuk, A.I., Kimura, J.I., Rybin, A.V., Yu, A., 2010. Geochemistry and petrogenesis of volcanic rocks in the Kuril island arc. Petrology 18, 489–513.
McDonough, W.F., Sun, S.S., 1995. The composition of the Earth. Chemical Geology 120, 223–253.
Mueller, P.A., Wooden, J.L., Nutman, A.P., 1992. 3.96 Ga zircons from an Archean quartzite, Beartooth Mountains, Montana. Geology 20, 327–330.
Nyman, M.W., Karlstrom, K.E., Kirby, E., Graubard, C., 1994. 1.4 Contractional orogeny in western North America: evidence from ca. 1.4 Ga plutons. Geology 22, 901–904.
Ojakangas, R.W., Morey, G.B., Southwick, D.L., 2001. Paleoproterozoic basin development and sedimentation in the Lake Superior region, North America. Sedimentary Geology 141–142, 319–341.
Pearce, J.A., Norry, M.J., 1979. Petrogenetic implications of Ti, Zr, Y, and Nb variations in volcanic rocks. Contributions to Mineralogy and Petrology 69, 33–47.
Pearce, J.A., Harris, N.B.W., Tindle, A.G., 1984. Trace element discrimination diagrams for the tectonic interpretation of granitic rocks. Journal of Petrology 25, 956–983.
Pickard, A.L., 2002. SHRIMP U–Pb zircon ages of tuffaceous mudrocks in the Brockman Iron Formation of the Hamersley Range, Western Australia. Australian Journal of Earth Sciences 49, 491–507.
Pickard, A.L., 2003. SHRIMP U–Pb zircon ages for the Palaeoproterozoic Kuruman Iron Formation, northern Cape Province, South Africa: evidence for simultaneous BIF deposition on Kaapvaal and Pilbara cratons. Precambrian Research 125, 275–315.
Pietranik, A.B., Hawkesworth, C.J., Storey, C.D., Kemp, A.I.S., Sircombe, K.N., Whitehouse, M.J., Bleeker, W., 2008. Episodic, mafic crust formation from 4.5 to 2.8 Ga: new evidence from detrital zircons, Slave craton, Canada. Geology 36, 875–878.
Price, R.C., Johnson, L.E., Crawford, A.J., 1990. Basalts of the North Fiji Basin: the generation of back arc basin magmas by mixing of depleted and enriched mantle sources. Contributions to Mineralogy and Petrology 105, 106–121.
Qu, X., Xu, X.W., Liang, G.L., Qu, W.J., Du, S.J., Jiang, N., Wu, H.P., Zhang, Y., Xiao, H., Dong, L. H., 2009. Geological and geochemical characteristics of the Mengxi Cu–Mo deposit and its constrain on tectonic setting of the Qiongheba magmatic arc in eastern Junggar, Xinjiang. Acta Petrologica Sinica 25, 765–776 (in Chinese with English abstract).
Regelous, M., Hofmann, A.W., Abouchami, W., Galer, S.J.G., 2003. Geochemistry of lavas from the Emperor Seamounts, and the geochemical evolution of Hawaiian magmatism from 85 to 42 Ma. Journal of Petrology 44, 113–140.
Rojas-Agramonte, Y., Kröner, A., Demoux, A., Xia, X., Wang, W., Donskaya, T., Liu, D., Sun, M., 2011. Detrital and xenocrystic zircon ages from Neoproterozoic to Palaeozoic arc terranes of Mongolia: significance for the origin of crustal fragments in the Central Asian Orogenic Belt. Gondwana Research 19, 751–763.
Rudnick, R.L., 1995. Making continental crust. Nature 378, 571–578.
Rudnick, R.L., Fountain, D.M., 1995. Nature and composition of the continental crust: a lower crustal perspective. Review of Geophysics 33, 267–309.
Sengör, A.M.C., Natal'in, B.A., 1996. Turkic-type orogeny and its role in the making of the continental crust. Annual Review of Earth and Planetary Science Letters 24, 263–337.
Sengör, A.M.C., Natal'in, B.A., Burtman, V.S., 1993. Evolution of the Altaid tectonic collage and Paleozoic crustal growth in Eurasia. Nature 364, 299–307.
Shu, L.S., Deng, X.L., Zhu, W.B., Ma, D.S., Xiao, W.J., 2011. Precambrian tectonic evolution of the Tarim Block, NW China: new geochronological insights from the Quruqtagh domain. Journal of Asian Earth Sciences 42, 774–790.
Simard, R.L., Dostal, J., Colpron, M., 2007. Rifting of a Mississippian continental arc system: little Salmon formation, Yukon–Tanana terrane, northern Canadian Cordillera. Canadian Journal of Earth Sciences 44, 1267–1289.
Sims, P.K., Van Schmus, W.R., Schulz, K.J., Peterman, Z.E., 1989. Tectono-stratigraphic evolution of the Early Proterozoic Wisconsin magmatic terranes of the Penokean orogen. Canadian Journal of Earth Sciences 26, 2145–2158.
Solomovich, L.I., 2007. Postcollisional magmatism in the South Tien Shan Variscan orogenic belt, Kyrgyztan: evidence for high-temperature and high-pressure collision. Journal of Asian Earth Sciences 30, 142–153.
Stacey, J.S., Kramers, J.D., 1975. Approximation of terrestrial lead isotope evolution by a two-stage model. Earth and Planetary Science Letters 26, 207–221.
Stern, R.A., Bleeker, W., 1998. Age of the world's oldest rocks refined using Canada's SHRIMP: The Acasta Gneiss Complex, Northwest Territories, Canada. Geoscience Canada 25, 27–31.
Stern, R.J., Bloomer, S.H., Martinez, F., Yamazaki, T., Harrison, M., 1996. The composition of back-arc basin lower crust and upper mantle in the Mariana Trough: a first report. The Island Arc 5, 354–372.
Su, C.Q., Jiang, C.Y., Xia, M.Z., Zhang, L., Ji, H.G., Guo, F.F., Liu, X.J., 2008. Zircon SHRIMP U–Pb dating from granite of the metamorphic complex system in Jueluotage tectonic belts and its geological significance. Acta Petrologica Sinica 24, 2789–2799 (in Chinese with English abstract).
Su, Y., Zheng, J., Griffin, W.L., Zhao, J., Tang, H., Ma, Q., Lin, X., 2012. Geochemistry and geochronology of Carboniferous volcanic rocks in the eastern Junggar terrane, NW China: implication for a tectonic transition. Gondwana Research 22, 1009–1029.
Sun, M., Yuan, C., Xiao, W.J., Long, X.P., Xia, X.P., Zhao, G.C., Lin, S.F., Wu, F.Y., Kröner, A., 2008. Zircon U–Pb and Hf isotopic study of gneissic rocks from the Chinese Altai: progressive accretionary history in the early to middle Paleozoic. Chemical Geology 247, 352–383.
Tang, H.F., Qu, W.J., Su, Y.P., Hou, G.S., Du, A.D., Cong, F., 2007. Genetic connection of Sareshike tin deposit with the alkaline A-type granites of Sabei body in Xinjiang: constraint from isotopic ages. Acta Petrologica Sinica 23, 1989–1997 (in Chinese with English abstract).
Taylor, S.R., McLennan, S.M., 1985. The Continental Crust: Its Composition and Evolution. Blackwell, Oxford pp. 697–719.
Thompson, A.G., Grambling, J.A., Karlstrom, K.E., Dallmeyer, B.D., 1996. Thermal evolution of Proterozoic middle crust during and following 1.4 Ga pluton emplacement, Manzano Mountains, New Mexico: pluton-enhanced 4 kb metamorphism, rapid decompression, and retrograde history. Journal of Geology 104, 583–598.
Vervoort, J.D., Blichert-Toft, J., 1996. Evolution of the depleted mantle: Hf isotope evidence from juvenile rocks through time. Geochimica et Cosmochimica Acta 63, 533–556.
Watson, M.P., Hayward, A.B., Parkinson, D.M., Zhang, Z.M., 1987. Plate tectonic history, basin development and petroleum source rock deposition onshore China. Marine and Petroleum Geology 4, 205–255.
Weaver, B.L., Tarney, J., 1984. Empirical approach to estimating the composition of the continental crust. Nature 310, 575–577.
Whitmeyer, S.J., Karlstrom, K.E., 2013. Tectonic model for the Proterozoic growth of North America. Geosphere 9, 220–259.
Wiedenbeck, M., Alle, P., Corfu, F., Griffin, W.L., Meier, M., Oberli, F., Vonquadt, A., Roddick, J.C., Speigel, W., 1995. Three natural zircon standards for U–Th–Pb, Lu–Hf, trace-element and REE analyses. Geostandard Newsletter 19, 1–23.
Windley, B.F., Allen, M.B., Zhang, C., Zhao, Z.Y., Wang, G.R., 1990. Paleozoic accretion and Cenozoic redeformation of the Chinese Tien Shan Range, Central Asia. Geology 18, 128–131.
Windley, B.F., Kröner, A., Guo, J.H., Qu, G.S., Li, Y.Y., Zhang, C., 2002. Neoproterozoic to Paleozoic geology of the Altai orogen, NW China: new zircon age data and tectonic evolution. The Journal of Geology 110, 719–737.
Windley, B.F., Alexeiev, D., Xiao, W.J., Kröner, A., Badarch, G., 2007. Tectonic models for accretion of the Central Asian Orogenic Belt. Journal of the Geological Society of London 164, 31–47.
Winter, J.D., 2001. An Introduction to Igneous and Metamorphic Petrology. Prentice Hall pp. 150–210.
Wong, K., Sun, M., Zhao, G., Yuan, C., Xiao, W., 2010. Geochemical and geochronological studies of the Alegedayi Ophiolitic Complex and its implication for the evolution of the Chinese Altai. Gondwana Research 18, 438–454.
Woodhead, J., Hergt, J., Shelley, M., Eggins, S., Kemp, R., 2004. Zircon Hf-isotope analysis with an excimer laser, depth profiling, ablation of complex geometries, and concomitant age estimation. Chemical Geology 209, 121–135.
Wu, F.Y., Yang, Y.H., Xie, L.W., Yang, J.H., Xu, P., 2006. Hf isotopic compositions of the standard zircons and baddeleyites used in U–Pb geochronology. Chemical Geology 234, 105–126.
Wu, F.Y., Zhao, G.C., Sun, D.Y., Wilde, S.A., Yang, J.H., 2007. The Hulan Group: its role in the evolution of the Central Asian Orogenic Belt of NE China. Journal of Asian Earth Sciences 30, 542–556.
Xia, L.Q., Xia, Z.C., Xu, X.Y., Li, X.M., Ma, Z.P., Wang, L.S., 2007. Magmatism in the Tianshan. Geological Publishing House, Beijing p. 350 (in Chinese).
Xiao, X.C., Tang, Y.Q., Feng, Y.M., Zhu, B.Q., Li, J.Y., Zhou, M., 1992. Tectonics in Northern Xinjiang and its Neighboring Areas. Geological Publishing House, Beijing p. 126 (in Chinese).
Xiao, W.J., Windley, B., Hao, J., Zhai, M.G., 2003. Accretion leading to collision and the Permian Solonker suture, Inner Mongolia, China: termination of the Central Asian Orogenic Belt. Tectonics 22, 1069–1089.
Xiao, W.J., Windley, B.F., Badarch, G., Sun, S., Li, J.L., Qin, K.Z., Wang, Z.H., 2004a. Palaeozoic accretionary and convergent tectonics of the southern Altaids: implications for the lateral growth of Central Asia. Journal of the Geological Society, London 161, 339–342.
Xiao, W.J., Zhang, L.C., Qin, K.Z., Sun, S., Li, J.L., 2004b. Paleozoic accretionary and collisional tectonics of the Eastern Tianshan (China): implications for the continental growth of central Asia. American Journal of Science 304, 370–395.
Xiao, W.J., Windley, B.F., Yan, Q.R., Qin, K.Z., Chen, H.L., Yuan, C., Sun, M., Li, J.L., Sun, S., 2006. SHRIMP zircon age of the Aermantai ophiolite in the North Xinjiang, China and its tectonic implications. Acta Geologica Sinica 80, 32–36.
Xiao, W.J., Han, C.M., Yuan, C., Sun, M., Lin, S.F., Chen, H.L., Li, Z.L., Li, J.L., Sun, S., 2008. Middle Cambrian to Permian subduction-related accretionary orogenesis of Northern Xinjiang, NW China: implications for the tectonic evolution of central Asia. Journal of Asian Earth Sciences 32, 102–117.
Xiao, W.J., Windley, B., Huang, B., Han, C., Yuan, C., Chen, H., Sun, M., Sun, S., Li, J., 2009a. End-Permian to mid-Triassic termination of the accretionary processes of the southern Altaids: implications for the geodynamic evolution, Phanerozoic continental growth, and metallogeny of Central Asia. International Journal of Earth Sciences 98, 1219–1220.
Xiao, W.J., Windley, B.F., Yuan, C., Sun, M., Han, C.M., Lin, S.F., Chen, H.L., Yan, Q.R., Liu, D.Y., Qin, K.Z., Li, J.L., Sun, S., 2009b. Paleozoic multiple subduction–accretion processes of the southern Altaids. American Journal of Science 309, 221–270.
Xiao, W.J., Huang, B., Han, C., Sun, S., Li, J., 2010a. A review of the western part of the Altaids: a key to understanding the architecture of accretionary orogens. Gondwana Research 18, 253–273.
Xiao, W.J., Mao, Q.G., Windley, B.F., Han, C.M., Qu, J.F., Zhang, J.E., Ao, S.J., Guo, Q.Q., Clevenn, R., Lin, S.F., Shan, Y.H., LI J.L., 2010b. Paleozoic multiple accretionary and collisional processes of the Beishan orogenic collage. American Journal of Science 310, 1553–1594.
Xiao, Y., Zhang, H., Shi, J., Su, B., Sakyi, P.A., Lu, X., Hu, Y., Zhang, Z., 2011. Late Paleozoic magmatic record of East Junggar, NW China and its significance: implication from zircon U–Pb dating and Hf isotope. Gondwana Research 20, 532–542.

Xiao, W.J., Windley, B.F., Allen, M.B., Han, C., 2013. Paleozoic multiple accretionary and collisional tectonics of the Chinese Tianshan orogenic collage. Gondwana Research 23, 1316–1341.

XJBGMR (Xinjiang Bureau of Geology and Mineral Resources), 2009. Geological map and explanatory text of Barkol, Xinjiang, China. Geological Survey Map L46C001003, scale 1:250,000.

Xu, X.W., Ma, T.L., 2004. Reply to the comment by Wen-Bin Zhu et al. on "Characteristics and dynamic origin of the large-scale Jiaoluotage ductile compressional zone in the eastern Tianshan Mountains, China". Journal of Structural Geology 26, 2337–2340.

Xu, X.W., Ma, T.L., Sun, L.Q., Cai, X.P., 2003. Characteristics and dynamic origin of a macro-scale ductile compressed zone formed in a Carboniferous back-arc basin, Jiaoluotage, Eastern Tianshan Mts., China. Journal of Structural Geology 25, 1901–1915.

Xu, P., Wu, F.Y., Xie, L.W., Yang, Y.H., 2004. Hf isotopic compositions of the standard zircons for U–Pb dating. Chinese Science Bulletin 49, 1642–1648.

Xu, X., He, G.Q., Li, H.Q., Ding, T.F., Liu, X.Y., Mei, S.W., 2006. Basic characteristics of the Karamay ophiolitic melange, Xinjiang, and its zircon SHRIMP dating. Geology in China 33, 470–475 (in Chinese with English abstract).

Xu, X.W., Jiang, N., Li, X.H., Qu, X., Yang, Y.H., Mao, Q., Wu, Q., Zhang, Y., Dong, L.H., 2013. Tectonic evolution of the East Junggar terrane: evidence from the Taheir tectonic window, Xinjiang, China. Gondwana Research 24, 578–600.

Yang, H.B., Gao, P., Li, B., 2005. The geological character of the Sinian Dalubayi ophiolite in the west Tianshan, Xinjiang. Xinjiang Geology 23, 123–127 (in Chinese with English abstract).

Yang, X.F., He, D.F., Wang, Q.C., Tang, Y., 2012a. Tectonostratigraphic evolution of the Carboniferous arc-related basin in the East Junggar Basin, northwest China: insights into its link with the subduction process. Gondwana Research 22, 1030–1046.

Yang, X.F., He, D.F., Wang, Q.C., Tang, Y., Tao, H.F., Li, D., 2012b. Provenance and tectonic setting of the Carboniferous sedimentary rocks of the East Junggar Basin, China: evidence from geochemistry and U–Pb zircon geochronology. Gondwana Research 22, 567–584.

Zhang, L.F., 1997. $^{40}Ar/^{39}Ar$ age of blueschists at Tangbale area from western Junggar, Xingjiang and its geological significance. Chinese Science Bulletin 42, 2178–2181 (in Chinese with English abstract).

Zhang, Y.Y., Guo, Z.J., 2008. Accurate constraint on formation and emplacement age of Hongliuhe ophiolite, boundary region between Xinjiang and Gansu Provinces and its tectonic implications. Acta Petrologica Sinica 24, 803–809 (in Chinese with English abstract).

Zhang, Z.M., Liou, J.G., Coleman, R.G., 1984. An outline of the plate tectonics of China. Geological Society of America Bulletin 95, 295–312.

Zhang, C., Zhai, M., Allen, M.B., Saunders, A.D., Wang, G.R., Huang, X., 1993. Implications of Palaeozoic ophiolites from Western Junggar, NW China, for the tectonics of central Asia. Journal of the Geological Society, London 150, 551–561.

Zhang, H.X., Niu, H.C., Terada, K., Yu, X.Y., Sato, H., Ito, J., 2003. Zircon SHRIMP U-Pb dating on plagiogranite from the Kuerti ophiolite in Altay, North Xinjiang. Chinese Science Bulletin 48, 2231–2235.

Zhang, H.Y., Niu, H.C., Sato, H., Shan, Q., Yu, X.Y., Ito, J., Zhang, Q., 2004. Late Paleozoic adakite and Nb-enriched basalt from Northern Xinjiang: evidence for the southward Subduction of the Paleo-Asian Ocean. Geological Journal of China Universities 10, 106–113 (in Chinese with English abstract).

Zhang, Z.C., Yan, S.H., Chen, B.L., Zhou, G., He, Y.K., Chai, F.M., He, L.X., Wan, Y.S., 2006. SHRIMP zircon U–Pb dating for subduction-related granitic rocks in the northern part of east Junggar, Xinjiang. Chinese Science Bulletin 51, 952–962.

Zhang, C.L., Li, X.H., Li, Z.X., Lu, S.N., Ye, H.M., Li, H.M., 2007. Neoproterozoic ultramafic-mafic-carbonatite complex and granitoids in Quruqtagh of northeastern Tarim Block, western China: geochronology, geochemistry and tectonic implications. Precambrian Research 152, 149–169.

Zhang, C.L., Li, Z.X., Li, X.H., Ye, H.M., 2009. Neoproterozoic mafic dyke swarms at the northern margin of the Tarim Block, NW China: age, geochemistry, petrogenesis and tectonic implications. Journal of Asian Earth Sciences 35, 167–179.

Zhang, Z.C., Zhou, G., Kusky, T.M., Yan, S.H., Chen, B.L., Zhao, L., 2009. Late Paleozoic volcanic record of the Eastern Junggar terrane, Xinjiang, Northwestern China: major and trace element characteristics, Sr–Nd isotopic systematics and implications for tectonic evolution. Gondwana Research 16, 201–215.

Zhang, Z., Deng, Y., Chen, L., Wu, J., Teng, J., Panza, G., 2013. Seismic structure and rheology of the crust under mainland China. Gondwana Research 23, 1455–1483.

Zhao, G., Cawood, P.A., Wilde, S.A., Sun, M., 2002. Review of global 2.1–1.8 Ga orogens: implications for a pre-Rodinia supercontinent. Earth-Science Reviews 59, 125–162.

Zhao, J., Liu, G., Lu, Z., Zhang, X., Zhao, G., 2003. Lithospheric structure and dynamic processes of the Tianshan orogenic belt and the Junggar basin. Tectonophysics 376, 199–239.

Zhao, G., Sun, M., Wilde, S.A., Li, S.Z., 2004. A Paleo-Mesoproterozoic supercontinent: assembly, growth and breakup. Earth-Science Reviews 67, 91–123.

Zheng, J.P., Sun, M., Zhao, G.C., Robinson, P.T., Wan, F.Z., 2007. Elemental and Sr–Nd–Pb isotopic geochemistry of Late Paleozoic volcanic rocks beneath the Junggar basin, NW China: implications for the formation and evolution of the basin basement. Journal of Asian Earth Sciences 29, 778–794.